University of Southern Queensland

Faculty of Engineering and Surveying

Optimisation of Flow through a Horizontal Spiral Baffled Filter

A dissertation submitted by

Mr Richard Michael John Ryan

Student No: 0050009002

In fulfilment of the requirements of

Bachelor of Engineering - Mechanical

ABSTRACT

This dissertation presents a solution to the phenomena of water channelling in a horizontally orientated sand filter. The aim is to find an optimal configuration of spiral baffle for a particular residence time and power input. A total of nine different spiral baffle geometries were considered.

The methodology for optimisation was to use computational fluid dynamics (CFD) software to study the flows in all nine geometries. A multiphase model was used to estimate the residence time of a volume fraction of fluid within the nine geometries. The residence time was then compared to the power input data to derive a solution.

Results show so far that by increasing the pitch the power requirement to drive the filter decreases. In addition to this as the baffle height is increased the power requirement increases also.

The spiral baffle represents a real solution to the problem of water channelling in a horizontal sand filter. One of the benefits of the spiral baffled filter could be the treatment of ground waters in developing countries. The advantage of the horizontal filter is that it could be made portable. With a portable sand filtration system the production of quality water could be achievable anywhere.

LIMITATIONS OF USE

University of Southern Queensland

Faculty of Engineering and Surveying

ENG4111 Research Project Part 1 &
ENG4112 Research Project Part 2

Professor Frank Bullen

Dean

Faculty of Engineering and Surveying
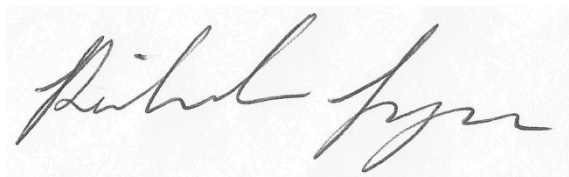
CERTIFICATION

I certify that the ideas, designs and experimental work, results, analyses and conclusions set out in this dissertation are entirely my own effort, except where otherwise indicated and acknowledged.

I further certify that the work is original and has not been previously submitted for assessment in any other course or institution, except where specifically stated.

Student Name: Richard Ryan
Student Number: 0050009002

_____
Signature

__26/10/2011_____
Date

ACKNOWLEDGEMENTS

This research was carried out under the principle supervision of Dr Ruth Mossad of University of Southern Queensland. Thank you for your support and guidance.

Special thanks to Daniel Grobbelaar and the team at LEAP Australia for their assistance in organising and providing software licensing for this project.

I would like to especially thank my wife Marissa and my two children Amelia and Isaac for their patience and support over the last 12 months whilst I completed this dissertation.

LIST OF FIGURES

LIST OF TABLES

TABLE OF CONTENTS

Chapter 1 **INTRODUCTION**

1.1 **Introduction**

Clean drinking water is a basic human need and is vital to the health and wellbeing of the community. Unfortunately, many people in developing countries do not have access to clean drinking water. The reasons for this are many but one is the economic cost of developing large scale water treatment facilities, often taken for granted by developed nations. It is hoped that through the application of modern technology a cheaper means of producing potable water can be developed. The spiral baffled horizontal sand filter, which was first proposed by Mossad & Aral (2010, pp. 25-37), is one such solution that could prove viable in the near future.

The spiral baffle offers a solution to the phenomena of water channelling which occurs in cylindrical horizontal sand filter. Water channelling occurs when a low resistance path is created through a porous media. In a cylindrical horizontal sand filter the water channel occurs along the top length of the filter. The water channel is marked by high flow velocities through the low resistance path. This high velocity water leads to very poor filtration and in some cases no filtration will occur. In order for horizontal sand filtration to become feasible a solution to water channelling must be found.

1.2 **Outline of Study**

The spiral baffle will be explored as a solution to water channelling in a horizontal sand filter. A total of nine different baffle geometries will be explored; each will have a different combination of baffle height and pitch. The spiral baffle models will be analysed using a numerical method and computational dynamics software (CFD).

As part of the CFD analysis the residence time of water in the filter will be approximated to give a comparative measure between models. The power loss across the filter will also be examined and compared to the baffle height and pitch in each model. It is hoped that an optimal solution or range of solutions will be obtained from the results.

1.3 **Background**

The problem of channelling of horizontal flow through a sand filter has been known for some time. This is the reason that horizontal sand filtration is not used in practice despite the known ability of sand filtration in water treatment.

Mossad and Aral (2010) have looked at various solutions to the problem of water channelling in horizontal water filters. Among these were baffles of vertical and spiral orientation, it was hoped these would reduce the problem of water channelling. Vertical baffle geometries were previously explored by Mead (2009) with various configurations being looked at.

The spiral baffle has been recognised as one of the more promising options, in terms of power and residence time (time taken for fluid to traverse filter) (Mossad & Aral 2010). However; only one configuration of spiral baffle geometry was considered during the initial investigation by Mossad and Aral (2010). For this reason the spiral baffle will now be considered further to study the effect that changes in geometry have on the flow characteristics.

1.4   **The Problem of Water Channelling**

The problem of channelling of fluids in porous media is noted in many areas of science and engineering. In the oil industry channelling of fluids in porous media has an adverse effect on the recovery of oil from wells (Salazar-Mendoza & Espinosa-Paredes 2009; Zhao 2011). Water channelling is quite simply the tendency of the water to flow along the path of least resistance. In a porous media the water channel could be an area of decreased density in relation to the remainder of the structure, or with sand it could be a different grade.

In a horizontally orientated sand filter the effect of water channelling occurs along the top of the filter. The settling occurs despite various methods being used to compact the sand once it is placed in the filter.

Water channelling can also occur at other layers in a porous medium. This has been observed in experiments of subsurface flows. In these experiments the inlet and outlet positions of a horizontal sand filter were varied to study the effects of water channelling (Suliman et al. 2006). The filter medium was also varied from a homogenous glass bead to layered packing of various sizes. Water channelling was noted to occur readily in the porous media of various sizes. This can be attributed to the variable resistance gradients created by size difference of the porous media grains.

The common element with channelling of fluid, regardless of the porous media, is the higher flow velocity. This high velocity flow, in relation to the rest of the porous media, is a real problem when the porous media is to be used for filtration. For effective filtration to occur it the fluid must pass through all the porous media at a steady flow rate. Water channelling causes the fluid to pass through only a portion at a high flow rate, leading to poor filtration.

1.5   **Research Objective**

The aim of this research is to study the effect that a variation in spiral baffle geometry has on the water channel in a horizontal sand filter. The residence time of water through various spiral baffle geometries will also be studied.

The general methodology that will be used is that of numerical modelling using CFD software. The water channel will be simulated using the software to produce a low resistance path. This low resistance path will be the same along the length of the filter in each model.

A thorough literature review of porous media and ways to model porous media will be under taken. Areas to be reviewed will be sand filtration methods that are currently used, both

vertical and horizontal. Filtration theory will be explored and its relationship to sand filtration. Ways of modelling flow through porous media using computational techniques will be investigated.

The data from the CFD modelling will be analysed with the aim of finding some optimal configuration of geometry. The power required at the various baffle heights and pitch will be used to compare results. The residence time calculated for a volume fraction of the fluid will also be used to try and establish some optimal configuration.

1.6   **Summary**

This dissertation will look at how flow through a horizontal sand filter is affected by changes to spiral baffle geometry. It is hoped that some optimal configuration of spiral baffle, in terms of power loss and residence time, can be found. It is expected that the spiral baffle will provide a good solution to the water channel effect within a horizontal sand filter. A review of the literature will show that the problem of water channelling within a horizontal filter produces poor filtration. It will also present a range of identified solutions to this problem.

Chapter 2 **LITERATURE REVIEW**

2.1   **Introduction**

This review will concentrate on water treatment methods using granular or sand type filters. A summary of the importance of water treatment will be given with a particular focus on the role of sand filtration. The general classifications of sand filtration will be examined and the important details of each method will be discussed.

The study of flow through a porous media is a complex process, many models exist that attempt to explain and predict the behaviour of this flow. Filtration can be explained using several of these models, the application and limitation of these models will be presented.

Filtration of fluid through a horizontal sand filter has several limitations these will be explored. In particular the limitations of horizontal sand filtration will be identified and solutions from past research will be discussed.

2.2   **Water Treatment with Sand Filtration**

Sand filtration of water is one of the oldest and most commonly used methods of producing potable water. The advantage with sand filtration is that it can be used to treat water that has a large variation in initial quality.

Generally, the treatment of potable water plays an important role in the health of the human population. Therefore sand filtration, in water treatment, contributes to the health of the population through a reduction in water borne bio-pathogens. The treatment of water, whilst important, is not a cheap process in terms of initial capital required for construction or ongoing running costs. For this reason water treatment by the lowest economic means is a major consideration in both developed and developing countries alike (Binnie et al. 2002).

Sand filtration is an important part in water treatment; improving the processes by which it filters water will allow it to be used more economically and efficiently. The process of water treatment by sand filtration involves the attachment of particles in the water to the porous media. There are several mechanisms of attachment to porous media that will be reviewed separately under filtration theory.

The use of the sand or granular filters for water treatment is very old and well-studied; however the majority of studies focus on the common vertical configuration of the sand filter. There have been many studies over the years in relation to the use and efficiency of vertical sand filters for the treatment of waste water (Ingallinella et al. 1998). Whilst the study of horizontal filtration is not as prevalent there are many studies of horizontal flow through a porous media. These studies focus on either flow through ground water aquifers or relate to the recovery of oil from porous media.

Sand filtration in the treatment of water is one of the most versatile methods of treatment. The quality of water that can be treated through sand filtration varies considerably, by

varying nothing more than the grain size of the sand. In addition to grain size there are several general classifications of sand filter each that have been created to be used at different points in the overall water treatment process. The selection of filter type will depend on the quality of the water being treated; the various types of sand filter will now be presented.

2.3   Types of Sand Filters

There are three main categories of sand filtration being; slow sand filters, rapid gravity filters and pressure filters. The slow sand filtration is one of the oldest forms of granular filtration, it's characterised by low loading rates and fine porous material. The slow sand filter primarily uses a layer of biological media that grows on the top layer of the sand. This biological layer treats the water initially before it passes through the remainder of the sand (Binnie et al. 2002).

Rapid gravity filters are the most common type of water filter used in water treatment. They are able to produce high quality water with a turbidity of 0.1 NTU from raw water, with a turbidity of between 5- 20 NTU. They are considered to work most efficiently when filtering raw water of turbidity 5 NTU (Binnie et al. 2002; Horvath 1994).

Pressure filters treat water by passing it through a granular filter media that is held in a pressure vessel. This type of filter is able to be used in line, with a pressurised pipe line for instance, without causing a major loss to the pressure within the pipeline. Pressure filters can be used either horizontally or vertically. The principle of operation of a pressure filter is the same as that of a rapid gravity filter (Binnie et al. 2002).

All three categories of sand filter are used in modern water filtration plants. The selection of a particular type over another depends on the turbidity of the water to be treated. The other consideration is the level of micro-biological material or pathogens needed to be removed. Horizontal sand filtration is receiving interest as an additional category used in modern water treatment; they show characteristic similar to rapid gravity and allow in-line use like pressure filters.

2.4   The Role of Horizontal Filters

Horizontal roughing filters have already been used in developing countries to treat water of high turbidity. Roughing filters have various grades of porous media arranged in several layers. They can be used in both the horizontal and vertical configuration. Up flow roughing filters have also been used with success in water treatment (Ingallinella et al. 1998).

Roughing filters are typically used as a first stage in the treatment of water; the filter media has a very course grain structure. Horizontal roughing filters are similar in structure to that of vertical sand filters in that they are housed in large concrete structures. As an alternative to this it has been proposed by Mossad & Aral (2010) that horizontal filtration could occur through pipes if modification is made to reduce water channelling.

An advantage of using a filter in a horizontal configuration is that it can be used to treat water directly pumped from ground water sites, for example mine waste water (Mossad & Aral 2010). A horizontal filter may not require the same energy that is needed for the more traditional vertical filters. But more importantly the capital outlay of infrastructure required for traditional vertical filters is substantial and beyond that of many developing nations (Skouras et al. 2007).

It is likely that a horizontal sand filter that can overcome the current limitations of water channelling would have many applications. The applications would not be limited to the treatment of mine waste water but would offer a low cost alternative water treatment in developing nations.

2.5   Models of Porous Flow

Probably one of the best known models of flow through porous media is Darcy's law. Darcy's law was derived from experiments performed by Darcy in 1856 on laminar flow through homogenous porous media. The mathematical relationship (Equ 2.5.1) derived from the experiment is:

$$Q = \frac{-KA(h_2 - h_1)}{h} \quad equ\ 2.5.1$$

In this equation Q is the volume flow rate, K is a constant that depends on the properties of the fluid and the porous media. In figure 2.5.1 the layout of Darcy's experiment can be seen, the height h is the characteristic length of the porous media. The difference in height, h_2-h_1, is the pressure across the media, A is the cross sectional area of the porous media.
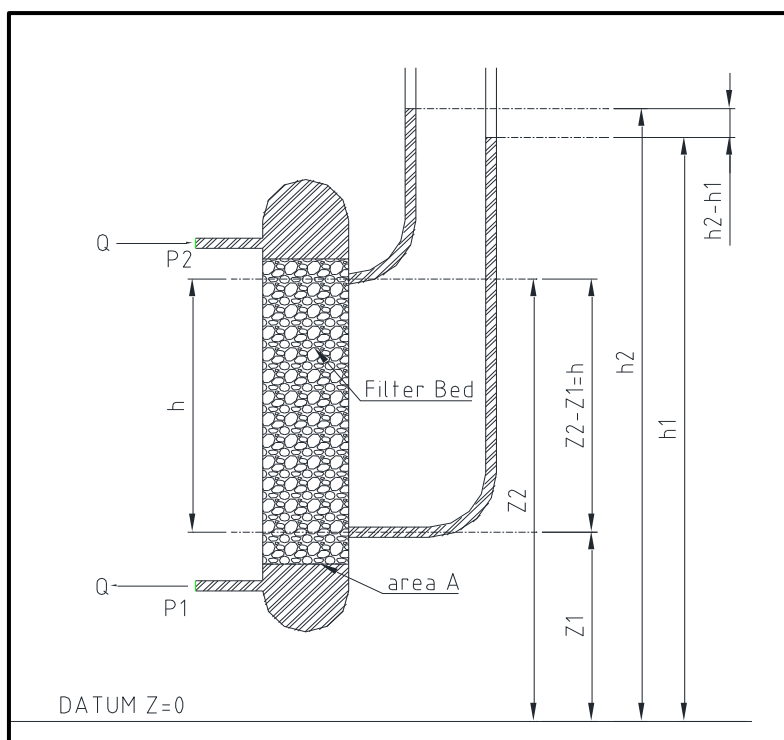
Figure 2.5.1: Darcy's experiment (Scheidegger 1963, p. 70).

Darcy's law has been tested many times showing that it is valid for a wide range of flow domains for liquids and gases. It has also been shown however that Darcy's law is invalid for flow of liquid at high velocity and for gas at both very low and very high velocity. It is believed that Darcy's law breaks down due to the onset of turbulence. This has led to the search for a critical Reynolds number to predict the transition from laminar to turbulent flow. However Scheideeger (1963, p. 169) believes that the breakdown of Darcy's law at high flow rates, is due more to the onset of inertial effects in laminar flow, than that of turbulence.

The constant K in Darcy's law as mentioned is related to the properties of the porous media. One of the most significant properties is that of the permeability of the porous media.

2.6   Porous media and Permeability

A general definition of porous media may be taken as a solid that contains numerous pores or voids. In order for flow to take place within a porous medium some of the pores must be interconnected somehow. The actual shape of these pores is a very difficult thing to define and it is even harder to model these pores mathematically.

The interconnection between porous media can be classified into several idealised types that describe the layout of pore spaces. For example the porous nature of sand in a filter has been classed by Scheideeger (1963) as a capillary, due to the hydrodynamic effect that the walls of the sand have on the fluid.

In equation 3.1 given previously, the constant K is related to the permeability of the porous media for a particular fluid. The constant K is therefore linked to the two properties; the liquid and the porous media. In order to make better use of Darcy's law the property of permeability needs to be defined. There are numerous equations that attempt to define the permeability of the porous media and therefore separate the effect of the liquid and the porous media that is contained in the constant K.

Another expression (Equ 2.6.1) that is related to permeability is porosity of the filter medium (Horvath 1994, pp. 173-4):

$$n = \frac{V_{pore}}{V_{total}} = \frac{V_{total} - V_{medium}}{V_{total}} \quad Equ\ 2.6.1$$

This is the ratio of the total pore volume, in the filter medium, to the total volume of the filter medium. Sand will typically have a porosity value of $n = 0.3 - 0.45$.

One of the challenges with the calculation of permeability or porosity in sand filters is the calculation of the size of sand particles. There are various ways to calculate the effective diameter of the sand particles and many models treat the particles as idealised spheres. This makes the calculation of porosity much simpler as it is almost impossible to accurately calculate the shape of sand particles due to the random nature of their shape (Horvath 1994, pp. 173-4).

2.7   **Filtration Theory**

Filtration through porous media is thought to occur by a combination of the following transport processes (Binnie et al. 2002; Horvath 1994):

- Interception
- Diffusion
- Hydrodynamic effect
- Inertia
- Attachment

These transport processes are shown in figure 3.2 which shows a suspended solid particle as it interacts with a grain of porous media.
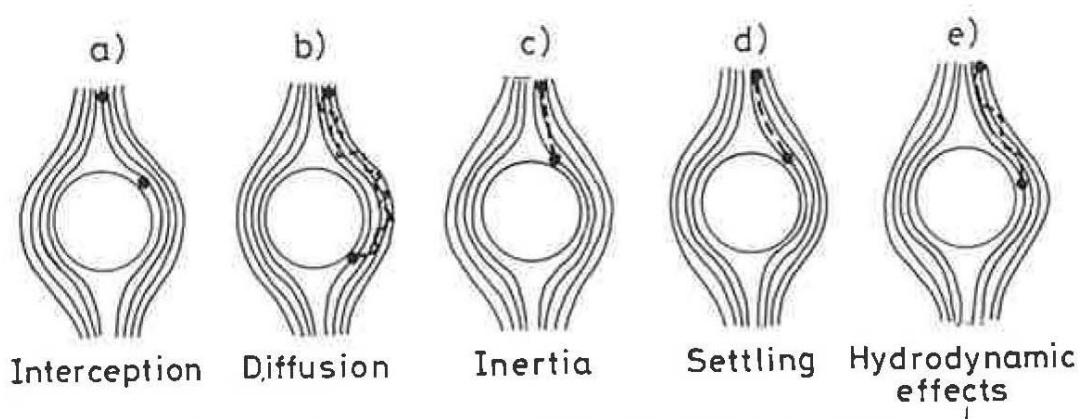
Figure 3.2: Various transport processes related to filtration (Horvath 1994, p. 178).

Interception shown figure 3.2a occurs when the particle in the fluid is intercepted by the filter medium. This is not to be confused with straining, which occurs when large particles are blocked by the filtrate. Rather interception is able to capture much smaller particles than would be possible with straining. Interception works by the adhesion of the particle to the surface of the filtrate medium.

Diffusion (figure 3.2b) is due to Brownian motion that affects very small particles, 1 micron or less, in the fluid flow. The path of the small particles is altered causing collision with the filtrate media. The number of collisions that occur has been said to be proportional to $(T/d_p d_m v)^{0.67}$, where T is equal to temperature, d_p being the diameter of the particle, d_m being the diameter of the filter media, and v being the velocity of the flow. The importance of this transport process is also thought to be low.

Hydrodynamic effect (figure 3.2e) or action occurs when a particle in the fluid passes a grain of filter media. The particle then rotates into the filter media as a result of velocity gradients. The particle will then attach to the filter media. This effect is not considered to be too significant.

Inertia effect (figure 3.2c) in water filtration basically involves the collision of particles with the filter media. This will occur as long as the particle is not overcome by the hydrodynamic effects that would see the particle turn and pass by the filter media.

Attachment (settling figure 3.2d) of particles to filter media occurs usually because of Van der Waal's forces between the filter media and the particle being filtered. This will occur provided that there are no electrostatic forces repelling the particle from the filter media. If particles are electrically charged then attachment will only occur if the electrostatic forces are opposite.

The various transport mechanisms given above will occur simultaneously, in varying degrees, in practical filtration. The relative importance of the individual transport mechanisms will vary depending on particle size being removed. It has been noted that the important transport mechanism for very small particles, in the order of $10^{-1}\mu m$, is diffusion. And for particles in the order of $1\mu m$ size the important transport mechanism is interception. Finally for larger particles, in order of $10\mu m$ and above, the predominant transport mechanism is straining (Binnie et al. 2002, p. 146). In summary interception and diffusion are of the most importance in practical filtration, the mechanism of straining is considered to lead to poor filtration efficiency.

2.8   Water Channelling in Porous Media

The channelling of fluids in porous media is experienced in many areas of science and engineering. In the oil industry channelling of fluids in porous media has an adverse effect on the recovery of oil from wells (Salazar-Mendoza & Espinosa-Paredes 2009; Zhao 2011). Water channelling is quite simply the tendency of the water to flow along the path of least resistance. In a porous media this could be an area of decreased density in relation to the remainder of the structure.

In a horizontally orientated sand filter the effect of water channelling occurs along the top of the filter. This was noted by Mossad & Aral (2010, p. 287) when investigating solutions to the water channelling in water filtration. The water channel is indicated by a small air gap that occurs when water is added to compacted filter sand.

Water channelling can also occur at other layers in a porous medium. This has been observed in experiments of subsurface flows. In these experiments the inlet and outlet positions of a horizontal sand filter were varied to study the effects of water channelling (Suliman et al. 2006). The filter medium was also varied from a homogenous glass bead to layered packing of various sizes. Water channelling was noted to occur readily in the porous media of various sizes. This can be attributed to the density gradients created by the size difference in the grains of the porous media.

Water channelling poses a real problem to the effectiveness of horizontal sand filtration. The effect of water channelling is the same regardless of its position in a porous media. The effect is that the water will flow at increased velocity to that of the rest of the flow.

2.9   **Summary**

Water treatment is an important part of the health and well being of society, sand filtration plays an important part in water treatment and therefore health. The delivery of treated water by the lowest economic means is an important priority for both developed and developing countries.

Several general classifications of sand filter are used in modern water treatment plants; horizontal sand filters are currently used as roughing filters. Horizontal sand filtration through pipes could be an economical alternative when a solution to the limitation of water channelling is found.

The most used equation that describes the behaviour of fluids through porous media is Darcy's law. It is valid for flows of fluid at low velocity and becomes invalid when the velocity becomes excessive. It is applicable at the velocities that are commonly used in water filtration.

In order to use Darcy's law in practice the permeability of the porous media must be modelled so that it can be applied to a range of fluids. The relationship between pores in sand filters is very complex; therefore idealised models are needed to describe the relationship.

Filtration through porous media relies on several attachment theories to explain the removal of particles from the fluid. The importance of the theory depends on the size of the particles that are to be removed by the porous media. Interception and diffusion are the most important theories used in modern water treatment.

Horizontal sand filtration through pipes is not currently possible due to the limitations created by the water channelling. Water channelling gives poor filtration efficiency due to the flow of fluid through the channel at high velocity.

Chapter 3 **METHODOLOGY**

3.1 **Introduction**

The methodology that will be used for this project will be to numerical model and optimise the layout of the spiral baffle using CFD software. Software simulation was used as it allowed for multiple variations of the spiral geometry to be checked in a fast and economical fashion.

The CFD analysis consists of several components needed to be able to successfully to model flow in a horizontal sand filter. The components are; the numerical method, the governing equations, creation of the geometry, modelling of the water channel region and calculation of the residence time.

3.2 **Numerical Methods for Porous Media**

For modelling flow through porous media the equation generally used is that derived from Darcy's law. As discussed earlier this law holds for low filtration rates with flows in the laminar region only. For turbulent flow through porous media other models must be used.

The Reynolds number can be used in order to determine the flow regime that could be expected from a given filter loading rate. The critical Reynolds number, that defines the transition from laminar flow to turbulent flow in porous media has been given as Rcrit =38 (Horvath 1994, p. 177). Some caution should be used when applying a critical Reynolds number as the value will vary depending on the theory of permeability used. Scheidegger (1963, pp. 158-60) reported a large discrepancy amongst authors in regards to the critical value of Reynolds number at which the Darcy equation would no longer hold. None the less the calculation for Reynolds number (Equ 3.2.1) is:

$$\text{Re} = \frac{vD\rho}{\mu} \quad \text{Equ 3.2.1}$$

However when the flow is through a porous media then the equation (Equ 3.2.2) changes to (Binnie et al. 2002, p. 141):

$$\text{Re} = \frac{vD\rho}{(1-f)\mu} \quad \text{Equ 3.2.2}$$

- f is the porosity of the media.
- D is the particle diameter.
- v is the velocity into the filter.
- μ is the viscosity.

This calculation will be used to check the flow regime through the filter prior to solver setup.

An alternative to the Reynolds number, which is reportedly more commonly used with filtration, is that of the Blake number (Horvath 1994, pp. 176-7).

The Blake number is essentially a modified Reynolds number with terms that take into account the nature of the porous media. The Blake number (3.2.3) is given by:

$$Re = \frac{vl}{v} = \frac{v_t R_h}{v} \quad \text{Equ 3.2.3}$$

With the hydraulic radius (Equ 3.2.4) equal to:

$$R_h = \frac{dn}{6(1-n)} \quad \text{Equ 3.2.4}$$

Using equation 3.2.4 in equation 3.2.3 gives:

$$Re = \frac{\frac{v_f}{n}\frac{dn}{6(1-n)}}{v} = Bl \quad \textit{Equ 3.2.5}$$

Which reduces to give a Blake number equation of:

$$Bl = \frac{dv_f}{6(1-n)v} = \frac{v_f}{Sv} \quad \text{Equ 3.2.6}$$

- v_f = filtration rate (m/h).
- l = thickness of the filter medium.
- d = particle diameter (mm).
- $v_t = v_f/n$
- n = pore volume.
- R_h = hydraulic radius.
- v = kinematic viscosity (mm2/s).

The term S in equation 3.2.6 is the specific surface area of the media in the filter per unit volume, this relationship is:

$$S = \frac{6(1-n)}{d_e} \; (m^2/m^3) \quad \text{Equ 3.2.7}$$

In order to use equation 3.2.2 the permeability must be calculated for the porous region. The permeability is calculated in FLUENT™(ANSYS FLUENT User's Guide 2010, p. 301) using the Blake-Kozeny equation (Equ 3.2.8) as follows:

$$\alpha = \frac{D_p^2}{150}\frac{\varepsilon^3}{(1-\varepsilon)^2} \quad \text{Equ 3.2.8}$$

This is similar to the equation (Equ 3.2.9) used by Mossad & Aral (2010, p. 288) for permeability calculations which was given as:

$$\alpha = \frac{D_p^2}{147}\frac{\varepsilon^3}{(1-\varepsilon)^2} \quad \text{Equ 3.2.9}$$

When solving porous media flow problems using FLUENT™ the pores of the media are considered to be 100% open. The software FLUENT™ defines the porosity as the open volume fraction of the media being used.

3.3   Governing Equations

The governing equations that are used in (ANSYS FLUENT User's Guide 2010) to model water flow through the porous media are the continuity and momentum equations. Given the assumption of incompressible laminar flow, constant viscosity, and the effects of gravity, the following equations can be derived:

$$\frac{\partial u}{\partial x} + \frac{\partial v}{\partial y} + \frac{\partial w}{\partial z} = 0 \quad Equ\ 3.3.1$$

$$u\frac{\partial u}{\partial x} + v\frac{\partial u}{\partial y} + w\frac{\partial u}{\partial y} = -\frac{1}{\rho}\frac{\partial p}{\partial x} + \mu\left(\frac{\partial^2 u}{\partial x^2} + \frac{\partial^2 u}{\partial y^2} + \frac{\partial^2 u}{\partial z^2}\right) + S_x \quad Equ\ 3.3.2$$

$$u\frac{\partial v}{\partial x} + v\frac{\partial v}{\partial y} + w\frac{\partial v}{\partial y} = -\frac{1}{\rho}\frac{\partial p}{\partial y} + \mu\left(\frac{\partial^2 v}{\partial x^2} + \frac{\partial^2 v}{\partial y^2} + \frac{\partial^2 v}{\partial z^2}\right) + S_y \quad Equ\ 3.3.3$$

$$u\frac{\partial w}{\partial x} + v\frac{\partial w}{\partial y} + w\frac{\partial w}{\partial y} = g - \frac{1}{\rho}\frac{\partial p}{\partial z} + \mu\left(\frac{\partial^2 w}{\partial x^2} + \frac{\partial^2 w}{\partial y^2} + \frac{\partial^2 w}{\partial z^2}\right) + S_z \quad Equ\ 3.3.4$$

The above equations represent the continuity (Equ. 3.3.1) and momentum equations (Equ. 3.3.2, 3.3.3, 3.3.4) and including the source term S for porous media. The source term, as given in the FLUENT™ user guide, gives a pressure drop caused by the resistance to flow due to the presence of the porous media (sand) that is proportional to the fluid velocity. The equation is given as:

$$S_i = -\left(\sum_{j=1}^{3} D_{ij}\mu v_j + \sum_{j=1}^{3} C_{ij}\frac{1}{2}\rho v_{mag} v_j\right) \qquad Equ\ 3.3.5$$

The first term in the above equation is Darcy's law, viscous loss term, and the second is the inertial loss term.

$$S_i = -\left(\frac{\mu}{\alpha} v_i + C_2 \frac{1}{2}\rho |v| v_i\right) \qquad Equ\ 3.3.6$$

In equation 5.3 above C_2 represents the inertia resistance factor, α is the permeability of the porous media. When the flow is laminar the inertial resistance term can be ignored which will leave Darcy's law to be included.

$$S_i = -\left(\frac{\mu}{\alpha} v_i\right) \qquad Equ\ 3.3.7$$

The source term in equation 5.4 now represents the pressure drop given in Darcy's law:

$$\nabla p = -\frac{\mu}{\alpha}\vec{v} \qquad\qquad Equ\ 3.3.8$$

The velocity that will be used in the model of the sand filter will be chosen after review of the literature and the past experiments of Mead (2009) and Mossad & Aral (2010). In Mead's work on the optimisation of vertical baffles in a horizontal sand filter a loading rate of 0.005m/s was used. This loading rate is similar to that used for the filtration of water in a rapid sand filter described by (Binnie et al. 2002). Mossad & Aral (2010, p. 288) on the other hand used 0.01m/s which is a much greater loading rate than that used for rapid sand filtration. However when considering the intended use that Mossad & Aral (2010, p. 287) had for the horizontal filter design it is not an unreasonable loading rate. Ultimately the design is intended to be used in line with a pump and will therefore be required to work at quite high loading rates.

3.4   **Model Geometry**

To be able to carry out CFD analysis on the spiral baffled filter then the geometry of each case must be modelled. The geometry for CFD needs to be of a good quality, this will make meshing of the models much easier. In this case ANSYS Design Modeller was used; the basic geometry was derived by creating a cylinder and removing the spiral baffle with a sweep feature by invoking the pitch command.

The spiral baffle variables that will be changed are the pitch of the baffle and the height of the baffle. The various combinations of baffle height and pitch that will be used are shown in table 3.2 below. A minimum of three baffle heights and pitches will be used; any less than this would not allow for any meaningful results as trends will not show up. More models would allow for even better resolution of results but time constraints dictate the use of no more than nine models.
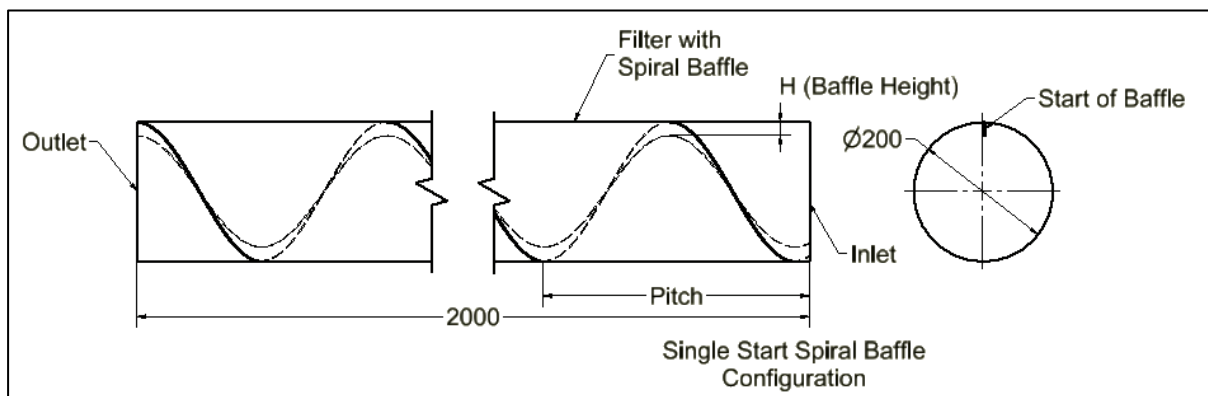
Figure 3.1: Spiral baffle filter geometry.

In addition to these models a plain filter was also modelled that has no baffle. The plain filter that will be designated SF10 is used as a base line and to look at the flow through a sand filter without baffles. The overall length and diameter of the geometry is the same as the other filters given in figure 3.1 above.

Model Numbers for Various Baffle Configurations			
Pitch	H=0.02m	H=0.04m	H=0.06m
0.25m	SF01	SF02	SF03
0.35m	SF04	SF05	SF06
0.45m	SF07	SF8	SF9

Table 3.2: Model number and dimension for each case studied

3.5   Modelling the Water Channel Region

Modelling the water channel is an important part of being able to model the behaviour of the flow in the horizontal sand filter. As mentioned in problem description the phenomena of water channelling is the very thing that makes horizontal sand filtration undesirable. For this reason the water channel region must be recreated in the model to be able to assess the ability of any proposed solution.

For the examination of the spiral baffle solution the following method has been used to create the water channel. The software allows the user to define a function (UDF) for any of the variables that are input into Fluent. The UDF that was used to model the water channel in this case has three assumptions.

The first assumption is that the water channel region occupies only the top 5% of the volume within the horizontal filter. This is the same assumption that has been used by Mossad & Aral (2010, p. 228) and Mead (2009) in their analysis of horizontal baffled filters. So for the sake of being able to compare results this assumption is being used here. This assumption would benefit from more empirical data relating to the exact nature of the water channel region at the top of the filter.
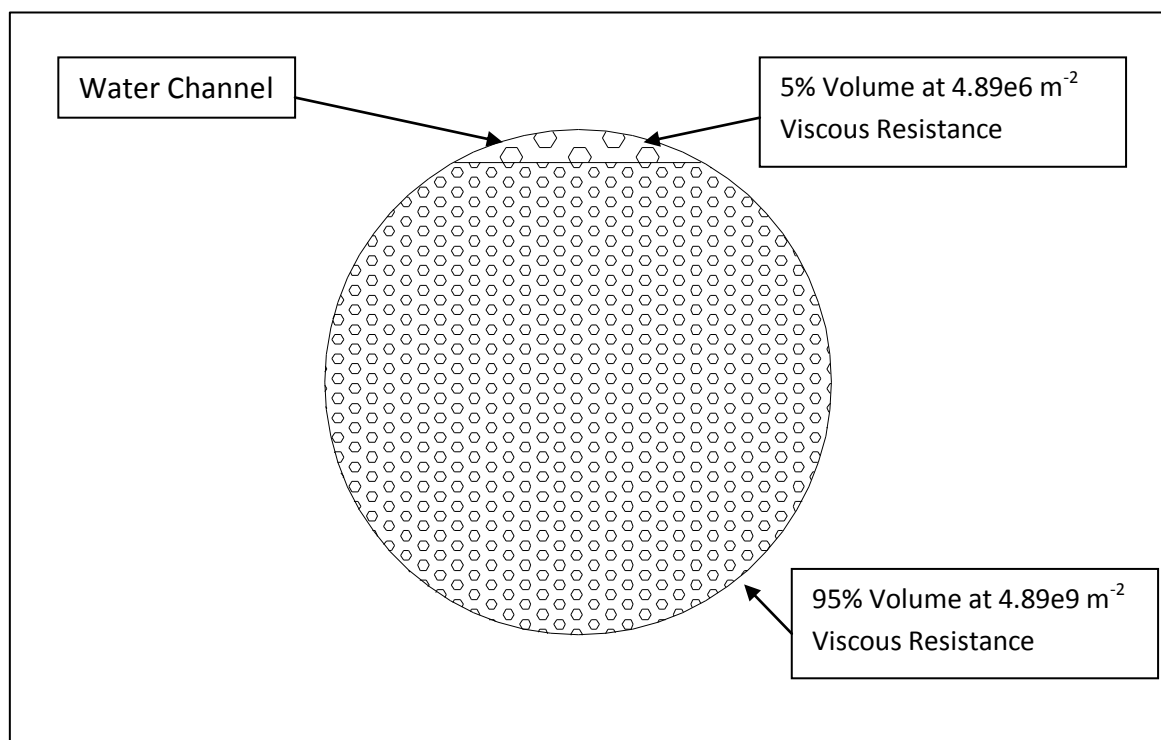
Figure 3.2: Filter cross section showing variation of viscous resistance as percentage of volume.

The second assumption that has been made in regards to the water channel region relates to the value of the low resistance path. The lower resistance has been created by making it three orders of magnitude lower than that of the viscous resistance. This approach is consistent with that used by both Mossad & Aral (2010) and Mead (2009) in their Analysis.

This approach is also recommended by the software manufacturer for the application (*ANSYS FLUENT User's Guide* 2010, pp. 228-9).

The third assumption is that there is a clear demarcation between the two resistance zones within the filter. The performance of the porous media, in this case sand, at this transition point may not behave as a porous material. For it to fit the definition of porous material it must be immoveable and the pores are continuous (Scheidegger 1963, pp. 5-8). However if a great enough velocity exists at the transition point then the sand may percolate within the low resistance zone. The transition zone assumption will therefore need to be validated at some stage in the future.

For the purpose of this analysis the aforementioned assumptions will be held and applied to the CFD models. The UDF that has been created for the viscous resistance will apply these assumptions to each of the equations within the solver. For details of the UDF refer to appendix C.

3.6   Calculating Residence Time

Calculation of residence time will be used to help optimise the spiral baffle geometries that have been modelled. The residence time will be used to give a relative comparison, between the selected geometries, of the time taken for a particle to traverse the filter.

The software offers several options for calculating the residence time; these options depend on the multiphase model being used. The method used with the Eulerian multiphase model is the used by Mossad & Aral (2010, p. 290). The method starts with the use of a two phase model, the second phase is named tracer and is given properties identical to that of the first phase which is water. A volume fraction of 10% of the tracer phase is defined at the inlet boundary of the spiral baffled filter. The modelled is then solved for a transient state and the facet average of the tracer at the outlet boundary is monitored. The flow time taken for the 10% of the tracer to appear at the outlet boundary is recorded as the residence time.

This method will allow for the comparison of each model in relation to the residence time, it does not however give any indication of the filtration efficiency. The reason for this is that the filtration attachment mechanisms, such as interception, are not accounted for. If the attachment mechanisms were accounted for then the model may well be suitable for very basic filtration efficiency calculations through the use of residence time.

3.7   Summary

All nine spiral baffle models will have the same velocity, porous and viscous resistance inputs. The value for the porosity that has been chosen was identified through the literature review. The porosity in each case will be 0.35 which is at lower end of the range given in the literature as between 0.35 to 0.45.

The viscous resistance, which will be discussed further in the solver setup, has been calculated from the porosity selected and from a porous media diameter. Using the equation

3.1 below the permeability is first calculated. The diameter of the media used for modelling porous media is 0.55mm in diameter which coincides to a grade of sand typically used in a rapid sand filter. The permeability is calculated thus:

$$\varepsilon = \text{Porosity}$$

$$D_p = \text{Diameter Porous Media}$$

$$\alpha = \text{Permiability}$$

Equation 3.1:

$$\alpha = \frac{D_p^2}{150} \frac{\varepsilon^3}{(1 - \varepsilon)^2}$$

$$\alpha = \frac{(0.55 \times 10^{-3})^2}{150} \frac{0.35^3}{(1 - 0.35)^2} = 2.0465 \times 10^{-10} \text{m}^2$$

The viscous resistance is the inverse of the permeability that has just been calculated, which is:

Equation 3.2:

$$\frac{1}{\alpha} = \frac{1}{2.0465 \times 10^{-10} \text{m}^2} = 4.89 \times 10^9 \text{m}^{-2}$$

The viscous resistance in equation 3.2 will be used to model the resistance in the sand of the horizontal filter. The area of the filter that is taken up by the water channel will be of a lower resistance however and will need to be set to a lower value.

Chapter 4 **COMPUTATIONAL FLUID DYNAMICS SETUP**

4.1 **Introduction**

An important part of the performance of a CFD analysis is the setup of the software to solve the given flow problem. In this case the setup must allow the methodology to be used to find the solution. The models and solver used will now be presented as they relate to the spiral baffle sand filter. The details of the meshing will also be presented here as it is closely related to the performance of the solvers in finding the solution.

4.2 **Boundary Conditions**

The boundary conditions used to model the spiral sand filters are the same for each case studied. The boundary conditions used to model the spiral sand filter include the following:

- Inlet
- Outlet
- Wall (Including baffle)
- Bulk (Internal area)

4.1.1 **Inlet Conditions**

The inlet boundary condition has been set to velocity and gauge pressure. The value of the velocity used is 0.01m/s which have been identified in the literature as rate similar to that used in a horizontal pressure filter.

The pressure at the inlet is considered to be gauge pressure zero which indicates atmospheric pressure.

4.1.2 **Outlet Condition**

The outlet condition for the spiral filter model is that of pressure gauge. The outlet of the spiral filter is considered to empty to atmosphere and therefore has a pressure of zero set.

4.1.3 **Wall and Baffle Boundary Conditions**

The wall of the spiral baffled sand filter is defined at the outer surface of the cylindrical filter body plus the baffle wall. The conditions at the wall are considered to be a non-slip condition.

All nine spiral baffle models will have the same velocity, porous and viscous resistance inputs. The value for the porosity that has been chosen was identified through the literature review. The porosity in each case will be 0.35 which is at lower end of the range given in the literature as between 0.35 to 0.45.

The viscous resistance, which will be discussed further in the solver setup, has been calculated from the porosity selected and from a porous media diameter. Using the equation

4.1 below the permeability is first calculated. The diameter of the media used for modelling porous media is 0.55mm in diameter which coincides to a grade of sand typically used in a rapid sand filter. The permeability is calculated thus:

$$\varepsilon = \text{Porosity}$$

$$D_p = \text{Diameter Porous Media}$$

$$\alpha = \text{Permiability}$$

Equation 4.1:

$$\alpha = \frac{D_p^2}{150} \frac{\varepsilon^3}{(1-\varepsilon)^2}$$

$$\alpha = \frac{(0.55 \times 10^{-3})^2}{150} \frac{0.35^3}{(1-0.35)^2} = 2.0465 \times 10^{-10} m^2$$

The viscous resistance is the inverse of the permeability that has just been calculated, which is:

Equation 4.2:

$$\frac{1}{\alpha} = \frac{1}{2.0465 \times 10^{-10} m^2} = 4.89 \times 10^9 m^{-2}$$

The viscous resistance in equation 4.2 will be used to model the resistance in the sand of the horizontal filter. The area of the filter that is taken up by the water channel will be of a lower resistance however and will need to be set to a lower value.

4.3   **Selection of CFD Model**

The selection of the model for solving the problem needed to consider the calculation of the residence time in addition to the pressure drop and the velocities. The residence time would be calculated using a volume fraction technique and this would determine the model used. A multiphase model would be used which would give access to various methods of calculating residence time for a volume fraction of water.

The Eulerian model was chosen as it uses a set of equations for each phase, these equations are coupled by a common pressure value. This method gives very accurate results but is also more computationally expensive, meaning the solution will take longer to achieve.

Some of the limitations of the Eulerian model are:

- The Reynolds stress turbulence model is not available.
- Particle tracking interacts with primary phase only.
- Inviscid flow is not allowed.
- Melting and solidification is not allowed.

Due to the flow through the filter being laminar none of the limitations affect the modelling of the spiral baffled filter.

4.4   Selection of Solver

The solver type that has been used the CFD analysis of the spiral baffle filters is a pressure based solver. This type of solver is suitable for incompressible flows so is well suited to the anticipated flow through the sand filter.

The other reason for the use of the pressure based solver is the multiphase models that are available with it. The multiphase model will be used in the residence calculation as discussed previously in the methodology.

The algorithm used for the "Phase Coupled SIMPLE" is adapted from the well known SIMPLE scheme and couples both phases with a single pressure. The SIMPLE scheme provides a way of calculating the pressure and velocity for the flow. This is required as the assumption of incompressibility of flow leaves no independent pressure equation in the governing equations (Tu et al. 2008, pp. 163-5).

The Phase Coupled SIMPLE scheme solves velocities in a segregated way that is coupled to each phase. The pressure correction is created from the momentum equations of each phase and the total continuity of the flow (*ANSYS FLUENT User's Guide* 2010, pp. 1190-3). The phase coupled scheme is robust and has been used for solving multiphase flows in ANSYS Fluent™ for many years.

4.5   Meshing of Spiral Filter

All the spiral baffled filters have been meshed using the same method; however each filter has a different number of nodes and elements. The variation in nodes and elements between the filter models is due to the variation in meshable area found in each geometry.

The elements used in the mesh are tetrahedrons which are applied using a patch conforming method available in the software.

Models	Elements	Nodes	Ave. Skewness	STD Deviation
SF01	1.257e6	3.235e5	0.26299	0.135
SF02	1.192e6	3.165e5	0.24466	0.137
SF03	7.655e5	2.317e5	0.24663	0.141
SF04	4.317e5	1.219e5	0.26021	0.132
SF05	2.884e5	84547	0.27521	0.138
SF06	2.456e5	75241	0.27959	0.146
SF07	2.523e5	81610	0.27875	0.138
SF08	5.669e5	1.775e5	0.21743	0.140
SF09	99320	37142	0.26565	0.151
SF10	101569	44026	0.17339	0.118

Table 4.1: Spiral baffled filter mesh details.

To increase the number of elements around the baffle region an inflation method was applied to the wall and baffle area. Increasing the number of elements in the wall and baffle region would allow for better resolution of the flow in these areas. This is a common technique that is applied to areas where the flow will change rapidly. It is considered to be more efficient computationally than applying the same fine mesh to the whole volume.

Chapter 5 **MODEL RESULTS**

5.1 **Introduction**

The results of the CFD analysis for each of the nine models will be presented focusing on the pressure drop, velocity profile and the residence time. An interpretation of the results will proceed and an attempt made to isolate an optimal configuration for the cases presented.

Presentation of the velocity profiles has been considered at two positions, the baffle mid-section and the water channel mid-section. The water channel mid-section is at a position half way between the pitch of the baffles (refer figure 5.1.1). This will give a plane that is equal distance between the baffles as they cut through the water channel. The baffle mid-section is directly aligned vertically with the baffle as it cuts through the water channel (refer figure 5.1.1).
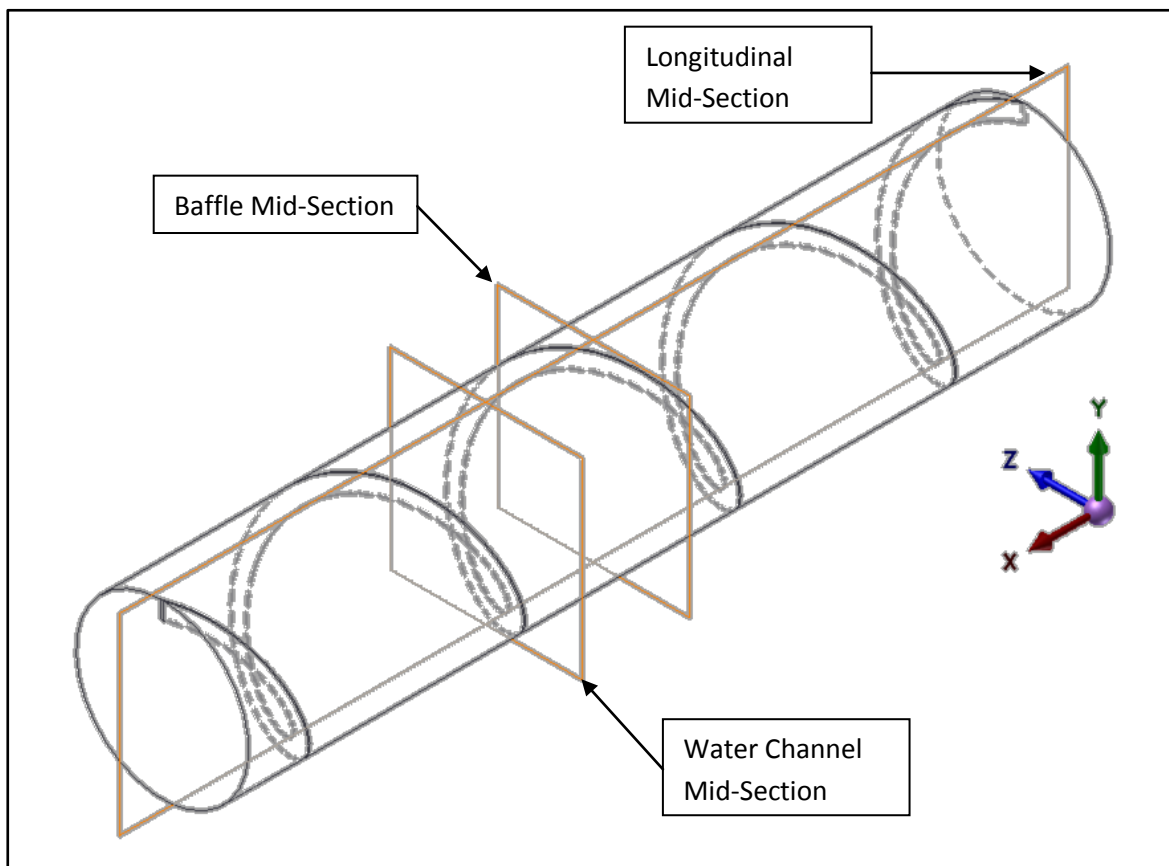
Figure 5.1.1: Orientation of planes used for reporting velocity.

These planes will differ from those used by Mossad & Aral (2010) in their comparison of various baffle options. Mossad & Aral(2010) used a section that was midway between the inlet and outlet of the filter. If this middle section was chosen for the spiral baffle models used in this investigation then the velocity profiles would change, due to the position of the plane in relation to the baffle (refer figure 5.1.2). The baffle position would vary for each different pitch, therefore making comparison more difficult between the various models.
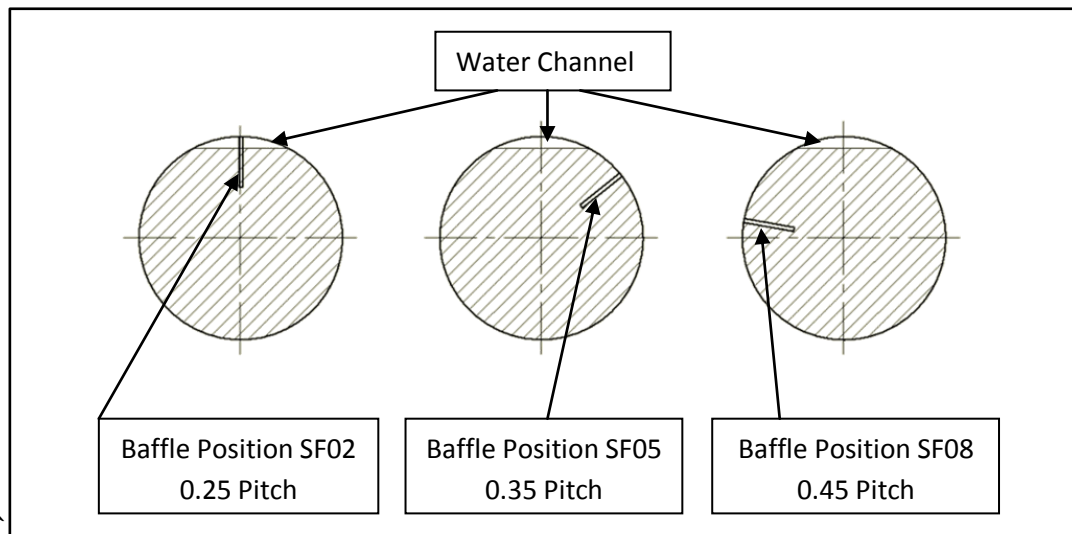
Figure 5.1.2: Baffle position at Mid-Section plane in relation to the water channel.

The pressure contours and velocity vectors will be presented in Appendix B along the longitudinal mid-section (figure 5.1.1) in each case. The baffle velocities will also be presented in Appendix B; the results are of less use in regards to comparing the various models due to the nature of the flow around the baffle.

The water channel midsection results give a good comparison between the various models, as the plane cuts the channel the same way in each case. The velocity results along the x, y and z axis will be presented for each case. A general discussion of the flow characteristics will be given as the behaviour of the flow in all models showed significant similarity.

5.2   General Flow Characteristics

The flow through all the models of spiral baffle showed similar characteristics. The most obvious characteristic is the high flow in the water channel region which can be seen in figure 5.2.1 below. Details of the magnitude of this flow will be given in following sections.

The flow around the baffle where it cuts through the water channel can also be seen in figure 5.2.1 below. In this case the flow is shown along the mid-plane of the filter; the flow pattern clearly shows the water flowing downward, under the baffle and up the other side.
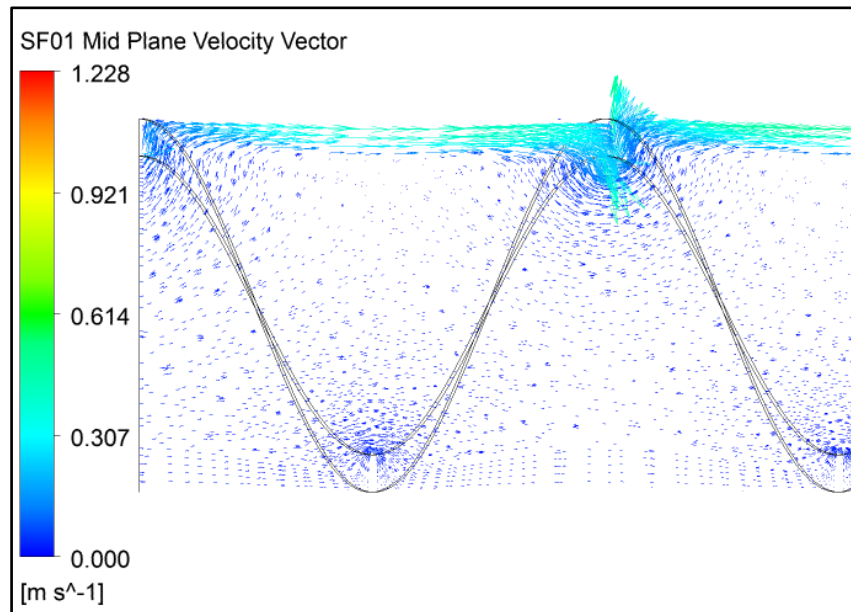
Figure 5.2.1: Velocity vectors along mid-plane, 0.25m pitch and 0.02m baffle height.

Looking at the flow from the top (figure 5.2.1, page 25) it can be seen that the velocity vectors at the top turn to follow the spiral baffle. This behaviour at the top of the filter is intuitive, more revealing than this however is the velocity vectors at the baffle section. The velocity at the baffle mid-section shows the behaviour of the flow at the base of the baffle (Appendix B) this can be seen in graph given in figure 5.2.3.
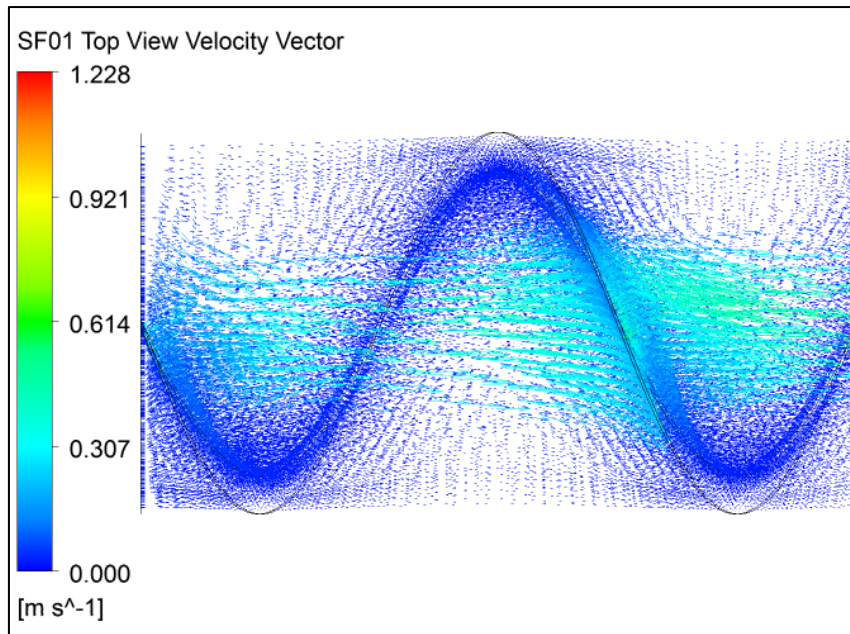
Figure 5.2.2: Velocity vectors top view, 0.25m pitch and 0.02m baffle height.

The velocity along the z-axis is in the negative direction, this is the opposite direction to that indicated by the velocity vectors at the top of the filter (figure 5.2.2). The reason for this is that the flow along the z-axis at the bottom of the baffle flows towards the low pressure side of the baffle. So at the bottom of the baffle it effectively flows backward as this is the shortest path to the lower pressure side of the baffle.
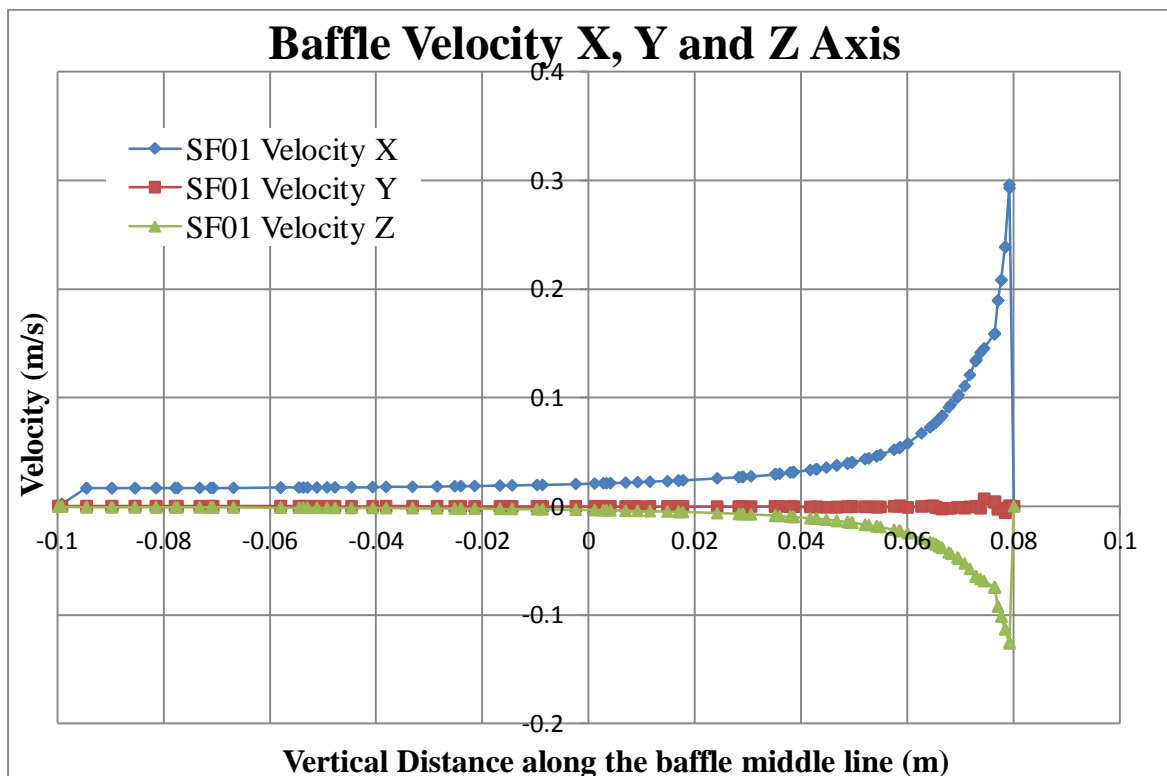
Figure 5.2.3: Velocity baffle mid-section of SF01, 0.25m pitch and 0.02m baffle height.

Velocity along the y-axis stayed fairly neutral until just below the baffle. At this point there was some rapid change between positive and negative values. The negative flows are a sign that the flow is moving downward, this is to be expected given the water is flowing around the baffle (refer figure 5.2.1).

All the filter models showed the same characteristic flow in terms of high velocity in the water channel and baffle flow (Appendix B). The velocity along each axis at the water channel mid-section will now be compared for the various configuration of pitch and baffle height.

5.3   **Water Channel Velocity Results.**

The velocity results in the water channel, for all the filter models, will be presented along each axis separately. The reason for this is the large variation in velocity between the x-axis and that of the y-axis and z-axis which makes plots difficult to interpret otherwise.

The velocity results will also be presented in table form showing the peak velocity and position as well as the average velocity.

5.3.1 **Results of Velocity X-Axis**

All the velocities along the x-axis at the water channel mid-section show the same pattern. As expected the velocity sharply increases as it enters the water channel at approximately 0.08m height (figure 5.3.2). At the bottom of the filter the velocity drops to zero at a position that corresponds to the height of the baffle for the particular filter model.

The peak velocities along the x-axis for each filter are given in table 5.3.1 below. From this it is clear that the position at which the peak velocity occurs within the water channel for each filter model is approximately the same.

The magnitude of the peak velocities is considerably higher than the inlet velocity of the filter which is 0.01m/s. This is not unexpected given that the resistance in the water channel is several orders of magnitude less than the remainder of the filter.

Model No.	Pitch	Baffle Height	Peak Velocity X	Position
SF01	0.25	0.02	0.49	0.095
SF02	0.25	0.05	0.40	0.097
SF03	0.25	0.08	0.38	0.095
SF04	0.35	0.02	0.63	0.094
SF05	0.35	0.05	0.52	0.095
SF06	0.35	0.08	0.48	0.095
SF07	0.45	0.02	0.57	0.091
SF08	0.45	0.05	0.66	0.096
SF09	0.45	0.08	0.58	0.095
SF10	n/a	n/a	0.83	0.096

Table 5.3.1: Peak velocities along x-axis and position for all filter models.

The Reynolds number for the average flow velocity in the channel section of the filter should be considered given the large increase in velocity. The characteristic length that will be used for the calculations is the depth of the low resistance channel. The formula used is:

$$Re = \frac{\rho v L}{\mu}$$

- $p = Density = 998.2 kg/m^3$
- $\mu = Viscocity = 0.001003 kg/m \cdot s$
- $L = Characteristic\ Length = 0.02m$
- $v = Peak\ Velocity = (m/s)$

Model No.	Pitch	Baffle Height	Average Velocity X	Reynolds Number
SF01	0.25	0.02	0.29	5798
SF02	0.25	0.05	0.30	5989
SF03	0.25	0.08	0.26	5207
SF04	0.35	0.02	0.43	8602
SF05	0.35	0.05	0.37	7319
SF06	0.35	0.08	0.35	6923
SF07	0.45	0.02	0.29	5769
SF08	0.45	0.05	0.46	9117
SF09	0.45	0.08	0.44	8777
SF10	n/a	n/a	0.66	13150

Table 5.3.2: Results of Reynolds number calculations at average channel velocity.

The calculated Reynolds number at the inlet velocity is:

$$Re = \frac{\rho v L}{\mu}$$

- $p = Density = 998.2 kg/m^3$
- $\mu = Viscocity = 0.001003 kg/m \cdot s$
- $L = Characteristic\ Length = 0.02m$
- $v = Peak\ Velocity = 0.01\ m/s$

$$Re = \frac{998.2 \times 0.01 \times 0.02}{0.001003} = 199$$

The difference between the peak Reynolds number and the value calculated at inlet velocity is considerable. The flow regime in the water channel should however remain in the laminar range for which it has been solved in Fluent™.
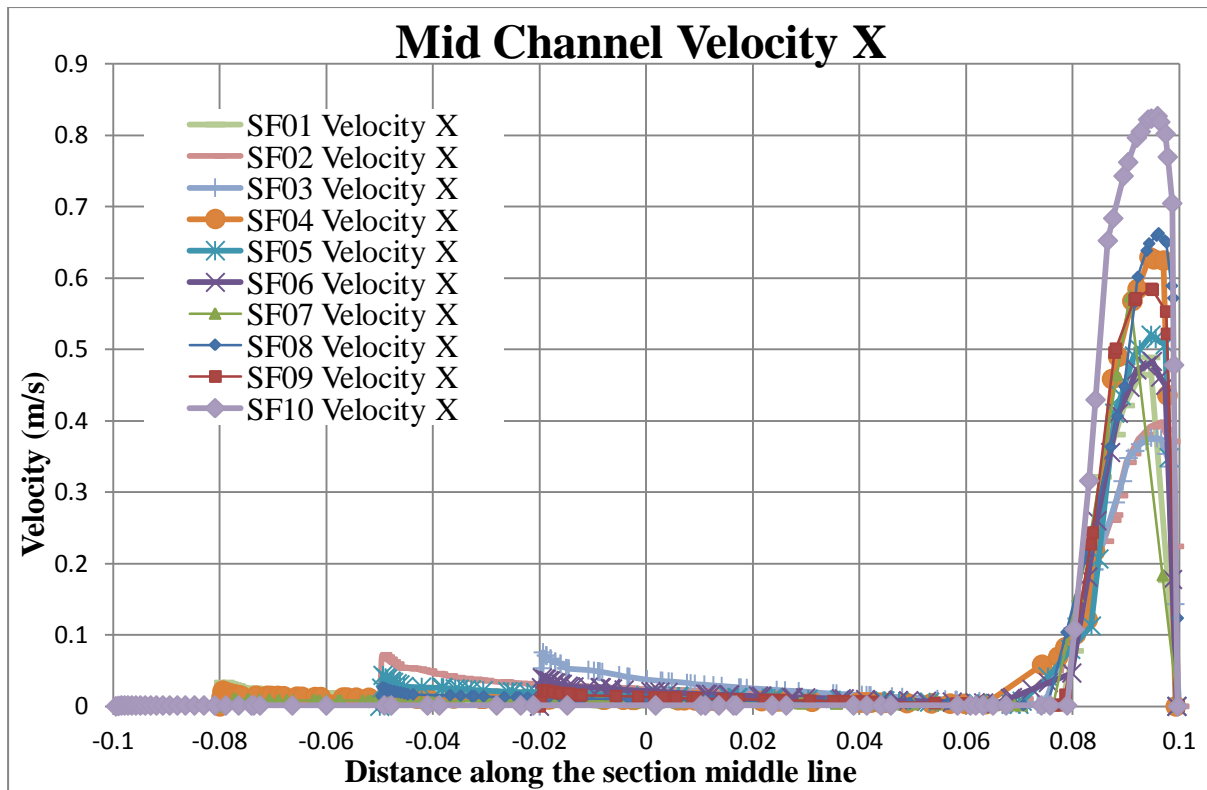
Figure 5.3.3: Mid water channel velocity along the x-axis for all filters.

5.3.2 **Results of Velocity Y-Axis**

The results of velocity along the y-axis (figure 5.3.5) at the mid-section of the water channel
show much lower velocities which is to be expected. From the velocity vectors (Appendix B)
it can be seen that the flow is predominately along the x-axis. The filter models show a mix
of negative and positive velocity in the water channel region. The negative velocity is an
indication of flow in a downward direction. This mix of positive and negative velocities is
more apparent when looking at tables 5.3.4 and 5.36.

Model No.	Pitch	Baffle Height	Peak Velocity Y	Position
SF01	0.25	0.02	-0.0058	0.090
SF02	0.25	0.05	0.0020	0.086
SF03	0.25	0.08	0.0026	0.099
SF04	0.35	0.02	-0.0018	0.091
SF05	0.35	0.05	-0.0036	0.092
SF06	0.35	0.08	-0.0058	0.087
SF07	0.45	0.02	0.0013	0.093
SF08	0.45	0.05	0.0108	0.090
SF09	0.45	0.08	-0.0042	0.088
SF10	n/a	n/a	-0.0046	0.086

Table 5.3.4: Peak velocities along y-axis in water channel for all filter models.

The position at which the peak velocity occurs in each filter is approximately the same and equates to a point that is midway in a vertical direction.
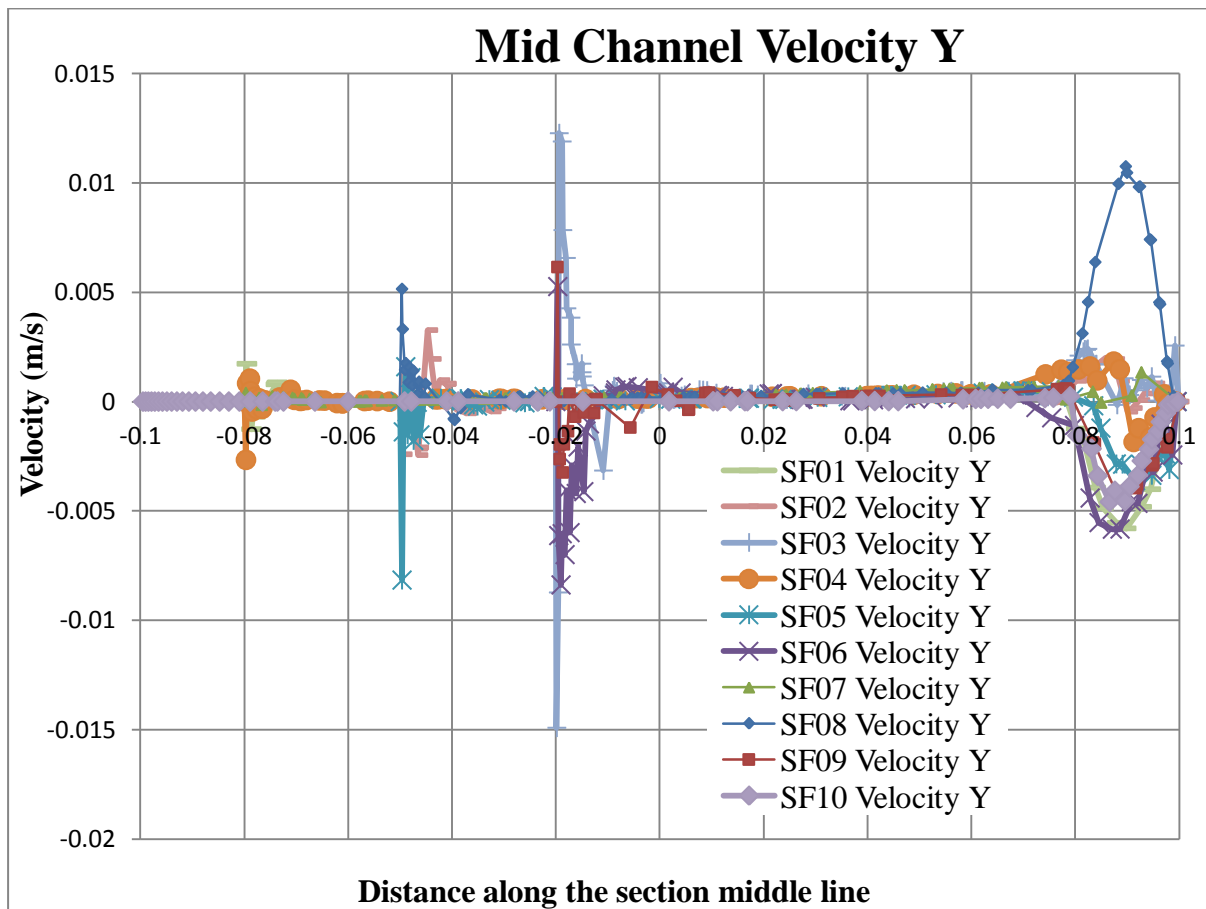

Figure 5.3.5: Mid water channel velocity along the y-axis for all filters.

The average velocities in the water channel (table 5.3.6) show no real pattern in relation to the pitch of baffle height. The average velocity in the water channel of the filter without the baffle, SF10, is small in magnitude and negative indicating a downward flow.

Model No.	Pitch	Baffle Height	Average Velocity Y
SF01	0.25	0.02	-0.0035
SF02	0.25	0.05	0.0006
SF03	0.25	0.08	0.0011
SF04	0.35	0.02	0.0001
SF05	0.35	0.05	-0.0023
SF06	0.35	0.08	-0.0035
SF07	0.45	0.02	0.0004
SF08	0.45	0.05	0.0054
SF09	0.45	0.08	-0.0027
SF10	n/a	n/a	-0.0021

Table 5.3.6: Average velocities y-axis in water channel for all filter models.

5.3.3 Results of Velocity Z-Axis

The velocity results along the z-axis are similar to the results from the y-axis velocities. The similarities are that there is a mix of both positive and negative velocities and that the magnitude of the velocities is low.
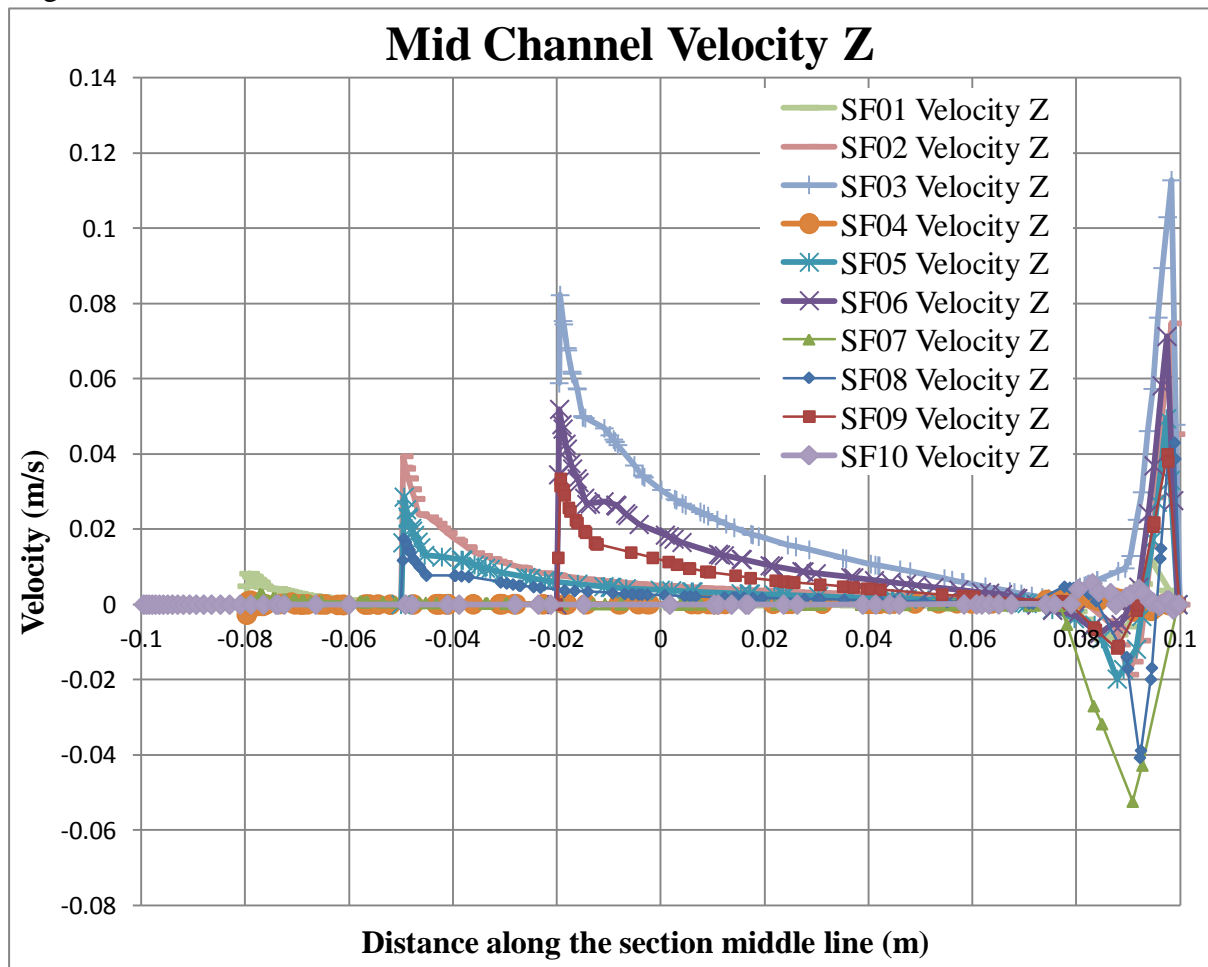

Figure 5.3.7: Mid water channel velocity along the z-axis for all filters.

The negative velocity in this case indicates that the flow is going in the opposite direction to that of the rotation of the spiral. The position for peak velocity (table 5.3.8) is higher amongst all the filter models, with the values being very close to the boundary layer.

Model No.	Pitch	Baffle Height	Peak Velocity Z	Position
SF01	0.25	0.02	0.011	0.098
SF02	0.25	0.05	0.075	0.097
SF03	0.25	0.08	0.113	0.098
SF04	0.35	0.02	0.028	0.097
SF05	0.35	0.05	0.049	0.097
SF06	0.35	0.08	0.071	0.097
SF07	0.45	0.02	-0.052	0.091
SF08	0.45	0.05	0.043	0.099
SF09	0.45	0.08	0.040	0.098
SF10	n/a	n/a	0.006	0.083

Table 5.3.8: Peak velocities along z-axis in water channel for all filter models.

The average velocity in the water channel is very low in magnitude, which is again expected due the predominance of the velocity along the x-axis. The average in most cases is much greater than the filter without a baffle. This is not too surprising as the flow in the spiral baffle filter should have a tendency to follow the curve of the baffle, therefore making flow along the z-axis much greater.

Model No.	Pitch	Baffle Height	Average Velocity Z
SF01	0.25	0.02	-0.0015
SF02	0.25	0.05	0.0127
SF03	0.25	0.08	0.0342
SF04	0.35	0.02	0.0016
SF05	0.35	0.05	0.0055
SF06	0.35	0.08	0.0166
SF07	0.45	0.02	-0.0308
SF08	0.45	0.05	0.0022
SF09	0.45	0.08	0.0076
SF10	n/a	n/a	0.0015

Table 5.3.9: Average velocities z-axis in water channel for all filter models.

5.4 Residence Time Results

The residence time results, presented in the graph below (figure 5.4.1), shows the residence time for each filter in seconds. The results show that at a pitch of 0.25m there is an increase in the residence time as the baffle height increases. Remembering that SF01 is of 0.02m, SF02 is 0.05m and SF03 is 0.08m in baffle height.

The first three filters show the pattern that is expected, as the resistance to flow increases so too does the time it takes for fluid to traverse the filter. The residence times of the other filters are in contrast to this expected behaviour.
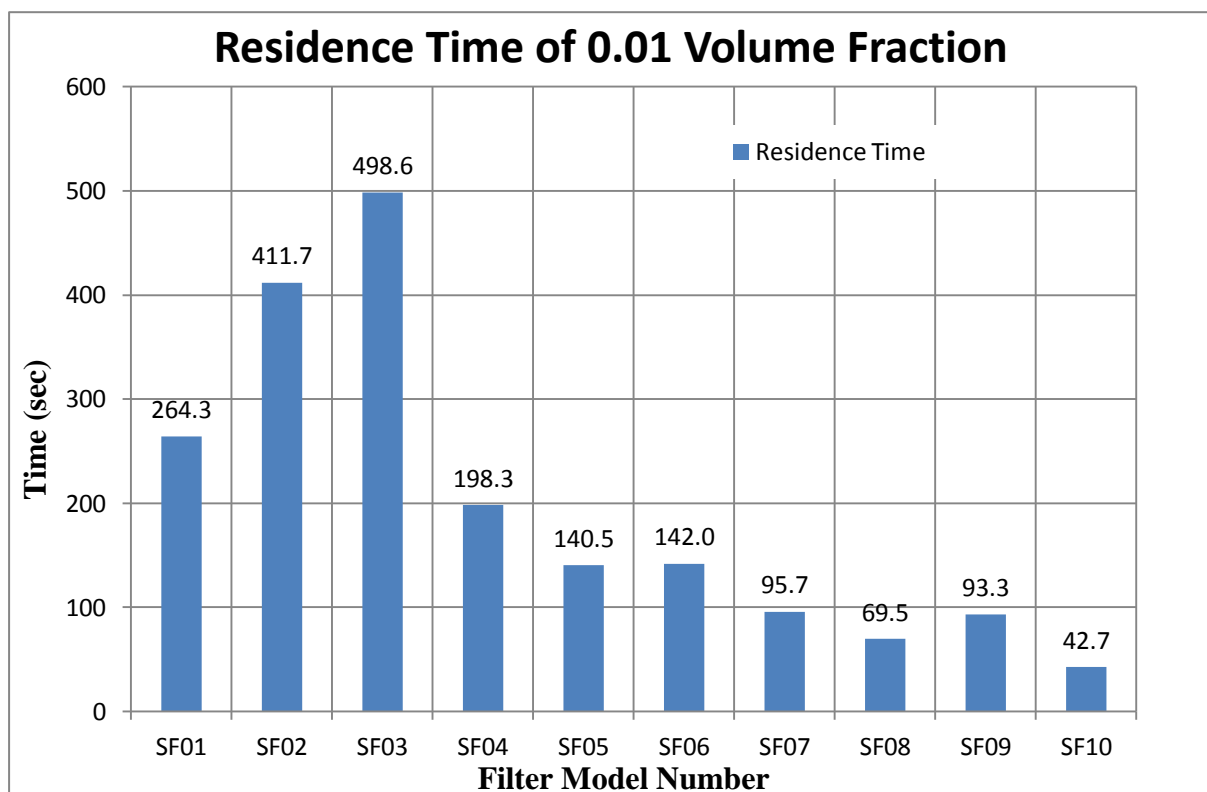

Figure 5.4.1: Change in pressure from inlet to outlet for various filter models.

For filters with a pitch of 0.35m the residence time drops from 198.3 seconds for a 0.02m baffle height to 140.5 seconds for the middle baffle height of 0.05m. The residence time for the 0.35m pitch between the 0.05m to the 0.08m baffle height actually increases slightly. This is the same pattern as that of the 0.045m pitch filters but is in contrast to that of the 0.25m pitch filters.

The increase in the residence time of the 0.25m filters as the baffle height increases makes sense. As the baffle height increases the resistance to flow increases and the water is pushed further down into the filter by the baffle. The reason for the decrease in residence time with increased baffle height of 0.35m and 0.45m pitch is unclear.

One possible explanation is the effect of increasing pitch; this may well exceed the effect that a change in baffle height has on the residence time. This would explain why there is a large drop between 0.25m pitch and 0.35m pitch and a continued drop of smaller magnitude to 0.45m pitch.

The other possible explanation is error in the method used to calculate the residence time. The volume fraction method used a transient solver and the time step was varied to different degrees throughout the solution process. The time steps were altered to reduce solution time but may well have introduced some error to the calculations.

To be able to establish if the data is revealing a trend, several models will need to be analysed at various pitch between 0.25m and 0.35m. This would give better resolution of results, at the moment there is a difference of nearly 300sec between SF03 and SF04. The time difference between the other models is far less than this indicating that the change in pitch is too great.

5.5 Pressure Drop Results

The pressure drop across the filter for each model can be seen in the graph below (figure 5.5.1), with the baffle height and pitch for each case given in table 5.5.2. The pressure drop increases as the baffle height increases for each case of pitch. Filters with the greatest baffle height of 0.08m are SF03, SF06 and SF09. These filters show the greatest pressure drop in comparison to filters of the same pitch.
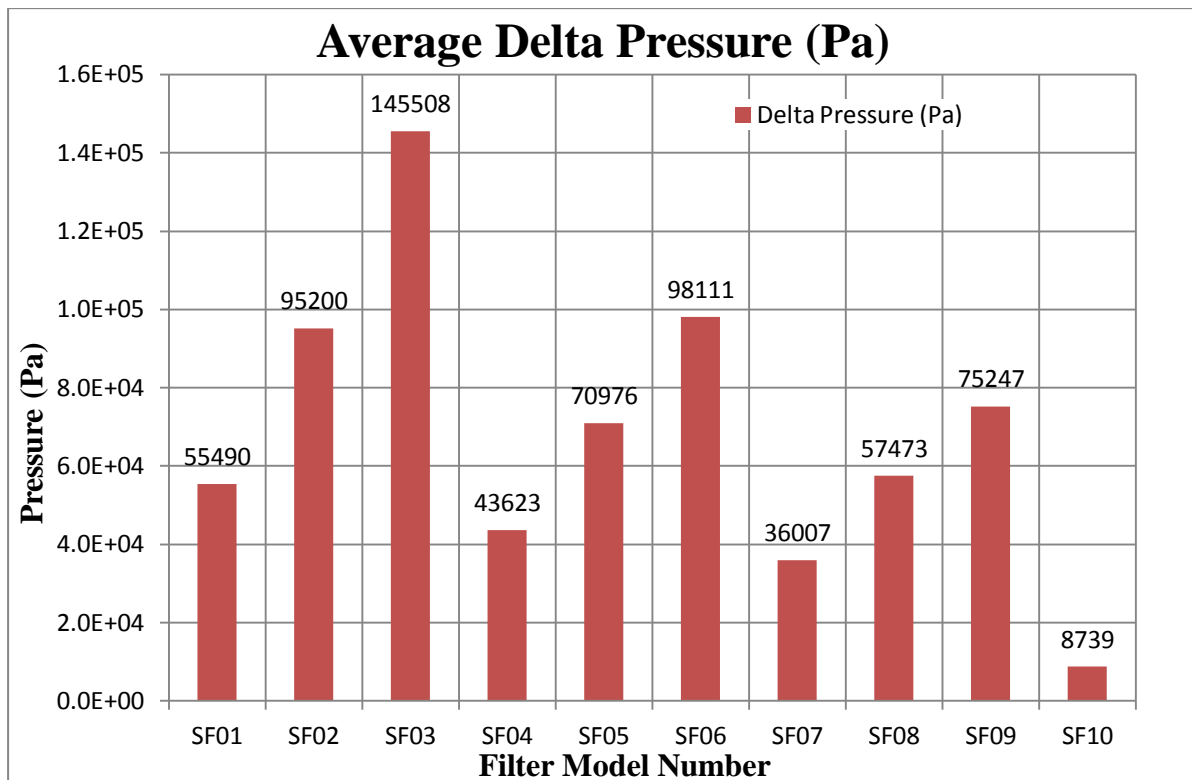

Figure 5.5.1: Change in pressure from inlet to outlet for various filter models.

As the pitch increases the pressure drop can be seen to decrease for all filters of the same baffle height. For example the filter models SF03, SF06 and SF09 show a decrease in pressure drop as the pitch goes from 0.25m, for SF03, to 0.45m for SF09.

Model Number	Pitch (m)	Baffle Height (m)
SF01	0.25	0.02
SF02	0.25	0.05
SF03	0.25	0.08
SF04	0.35	0.02
SF05	0.35	0.05
SF06	0.35	0.08
SF07	0.45	0.02
SF08	0.45	0.05
SF09	0.45	0.08
SF10	n/a	n/a

Table 5.5.2: Filter model numbers showing pitch and baffle height.

The significance of the pressure drop across the filters is apparent when the change in pitch and the change in height are considered separately.
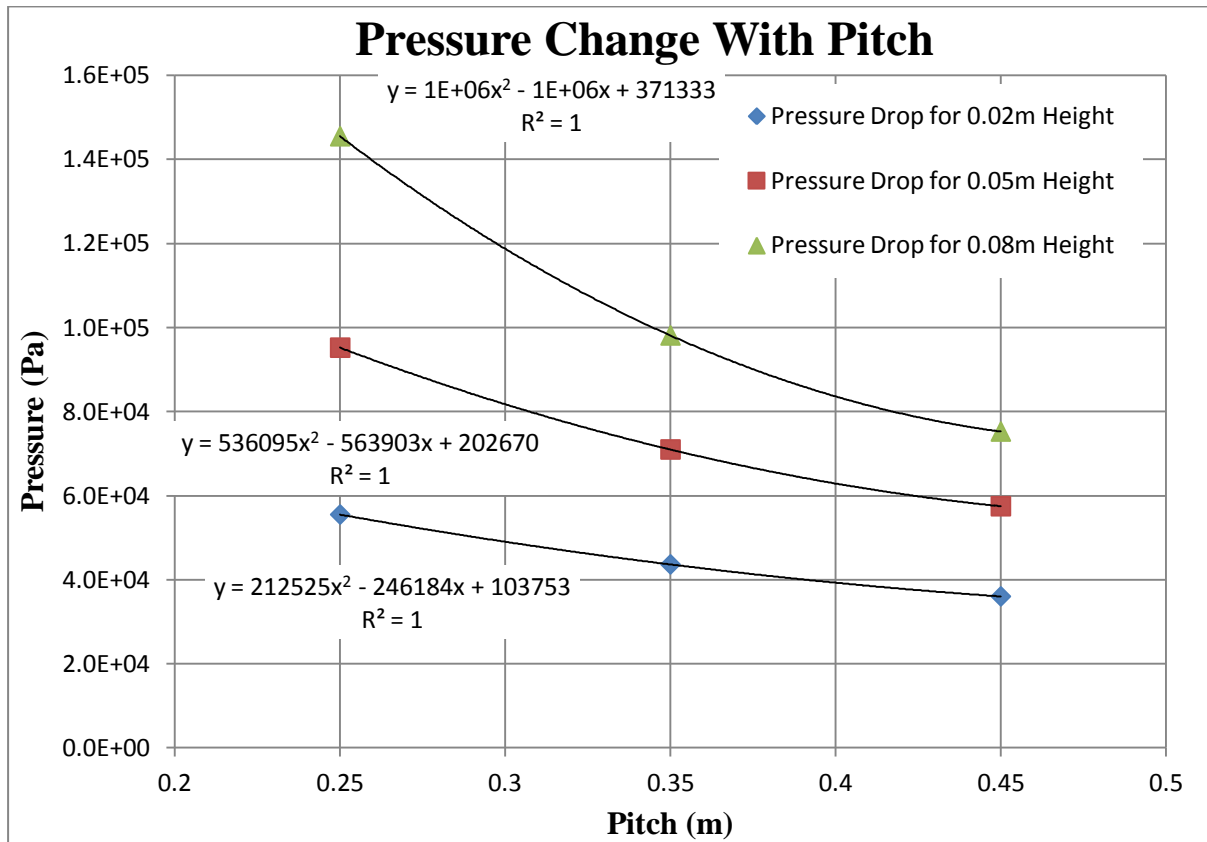

Pressure Change With Pitch

$y = 1E+06x^2 - 1E+06x + 371333$
$R^2 = 1$

$y = 536095x^2 - 563903x + 202670$
$R^2 = 1$

$y = 212525x^2 - 246184x + 103753$
$R^2 = 1$

- ◆ Pressure Drop for 0.02m Height
- ■ Pressure Drop for 0.05m Height
- ▲ Pressure Drop for 0.08m Height

Pressure (Pa)

Pitch (m)

Figure 5.5.3: Change in pressure as pitch increases at different baffle heights.

In figure 5.5.3 the pitch is varied for all three cases of baffle height. In each case as the pitch increases the pressure drops for the same baffle height.

In a similar fashion the baffle height was varied and the pressure change plotted for each case of pitch. This can be seen in figure 5.5.4 on the following page. As the baffle height is increased from 0.02m through to 0.08m the pressure increases for each case of filter pitch.
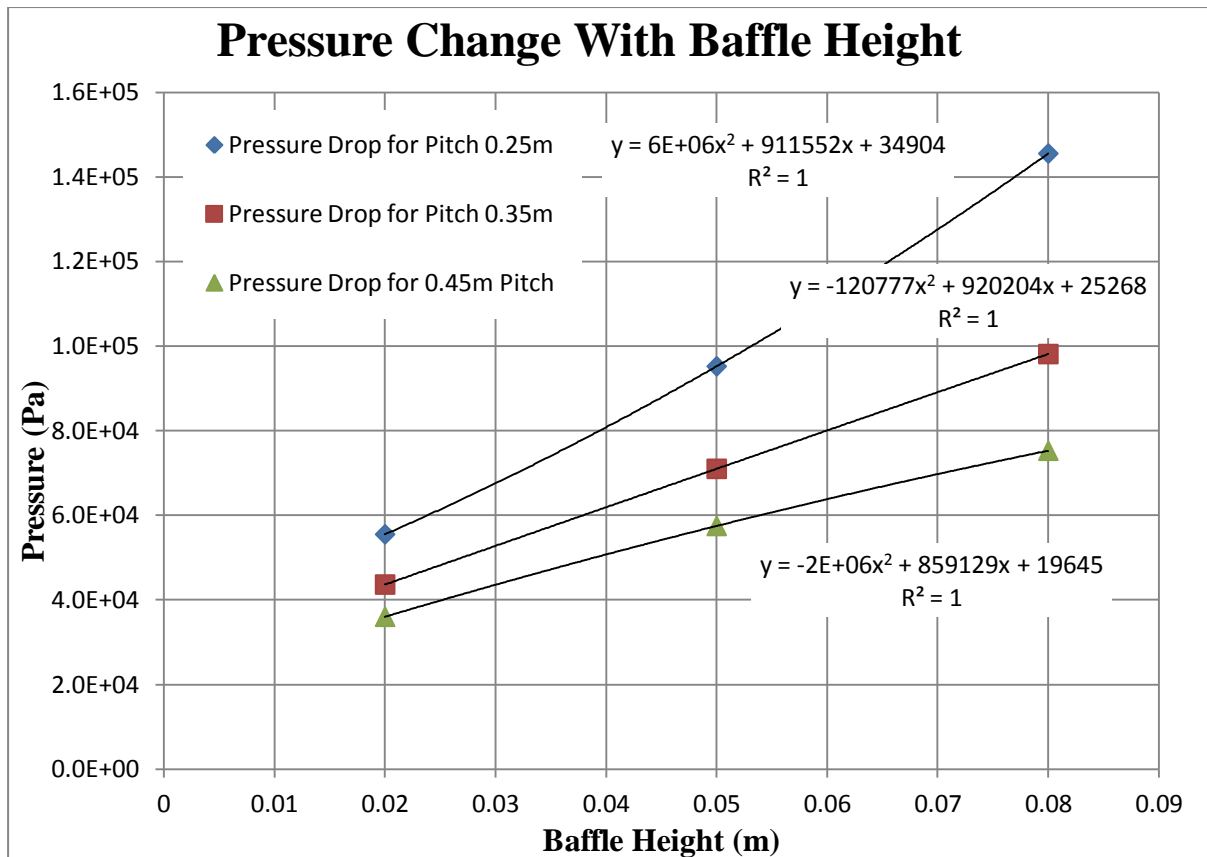
Figure 5.5.4: Change in pressure as baffle height increases at different baffle heights.

In each case the pressure drop is much greater than the filter without a baffle, SF10. The only resistance in SF10 is that of the porous media and so can be considered as the base line for all other models.

The change in pressure with pitch and baffle height mean that there are many possible combinations of baffle height and pitch that could give the same pressure drop. This will be discussed further when the subject of optimisation is discussed.

5.6   **Filter Power Input Calculations**

The power input required by each filter is to be used to compare results and for optimisation in regards to residence time. The power in watts will be calculated for each filter model using the volume flow rate and pressure drop as follows:

$$P = \Delta p \times Q$$

- $P = power\ in\ watts$
- $\Delta p = pressure\ drop\ (Pa)$
- $Q = volume\ flow\ rate\ (m^3/s)$

The results of the power input calculation for each filter model are given in table 5.7.1 below.

Model Number	Δp (Pa)	Q (m³/s)	P (W)
SF01	5.55E+04	3.12E-04	17.32
SF02	9.52E+04	3.12E-04	29.67
SF03	1.46E+05	3.10E-04	45.17
SF04	4.36E+04	3.12E-04	13.60
SF05	7.10E+04	3.10E-04	22.02
SF06	9.81E+04	3.09E-04	30.31
SF07	3.60E+04	3.12E-04	11.22
SF08	5.75E+04	3.12E-04	17.91
SF09	7.52E+04	3.09E-04	23.23
SF10	8.74E+03	3.12E-04	2.73

Table 5.6.1: input power calculations for the various filter models.
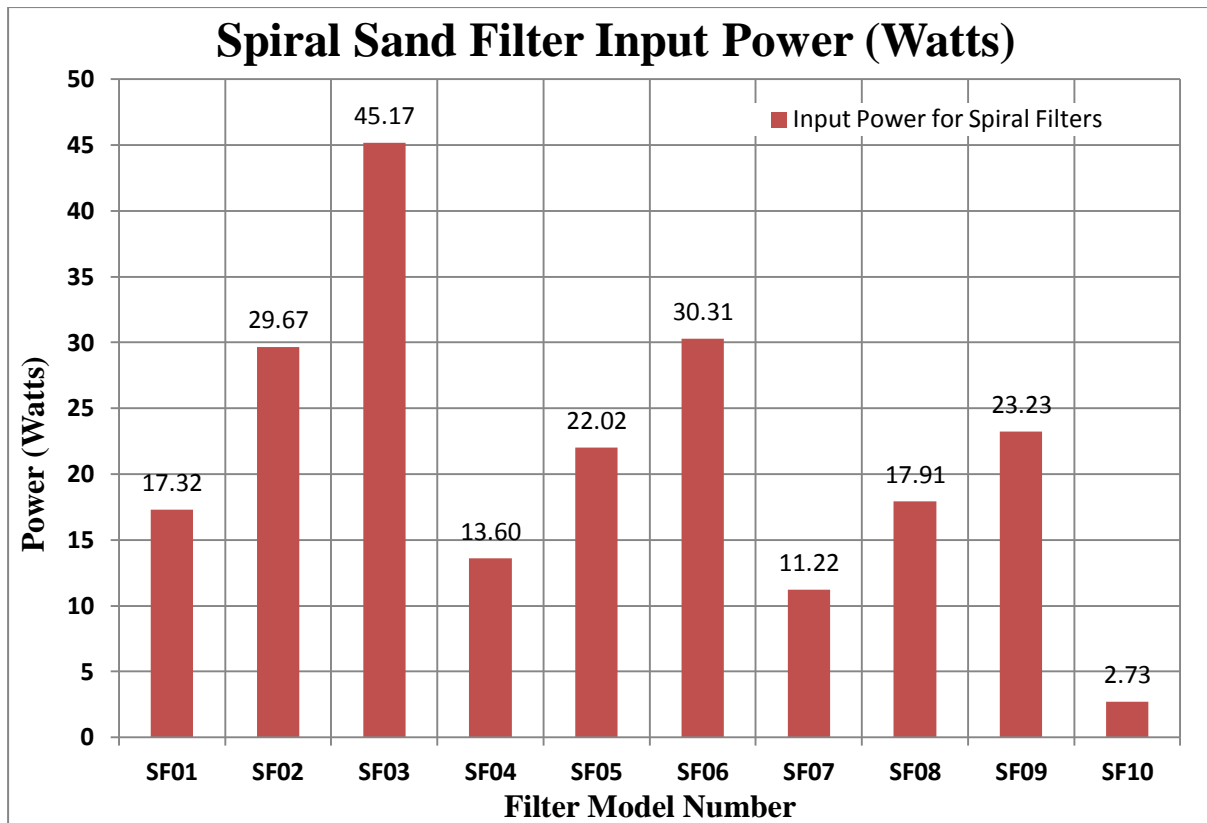
Figure 5.6.2: Chart showing spiral filter input power for various models.

The chart in figure 5.6.2 shows a definite pattern in regards to the change in power required for the various filters. Looking at a particular baffle height such as 0.02m height which covers models SF01 (pitch 0.25), SF04 (pitch 0.35) and SF07 (pitch 0.45) you can see the power required drops as pitch increases.

Focusing on the change in baffle height as the pitch remains the same the inverse occurs. For example models SF01 (Baffle 0.02m), SF02 (Baffle 0.05m) and SF03 (Baffle 0.08m) the power required increases from 17.32 Watts for SF01 to 45.17 Watts for SF03. As expected all filter models require more power input than the non-baffled filter SF10.

These changes in power required make sense when considering the baffles and the resistance that they have to flow through the filter. The resistance to flow in relation to the pitch will decrease as the pitch increases. This is due to the decreasing angle the baffle takes to the flow along the x-axis. The change in angle of the baffle in relation to the x-axis can be seen in figure 5.6.3 below showing SF01 of pitch 0.25m and SF07 of 0.45 pitch.
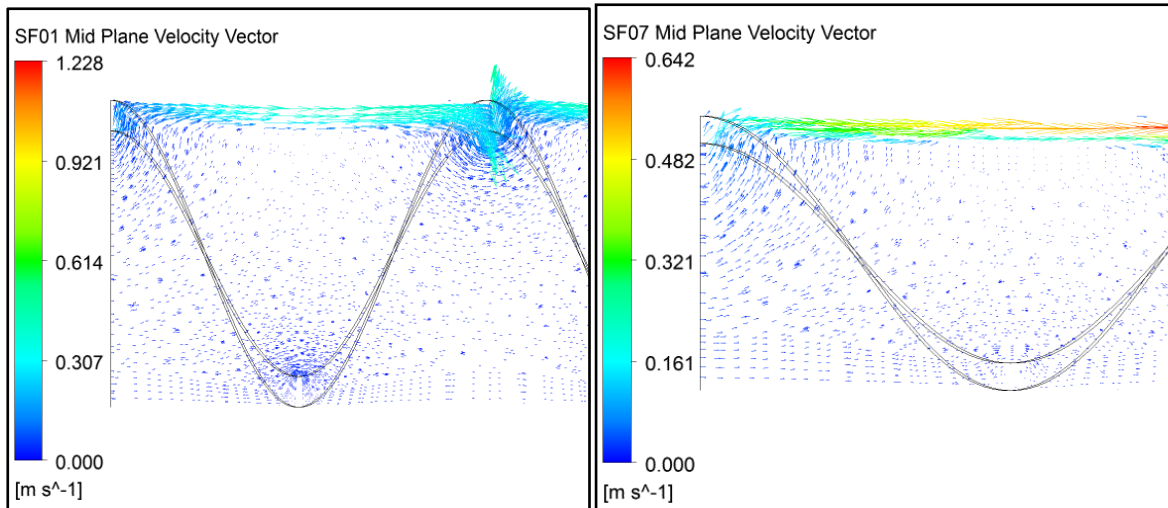
Figure 5.6.3: Spiral baffle SF01 of 0.25m pitch compared to SF07 of 0.45m pitch.

The resistance will increase as the baffle height increases as obstruction to the flow will be greater for the larger baffle height. This can be visualised by examining the velocity vectors in figure 5.6.4 which shows SF01 and SF03 which are at the extremes of baffle height for a pitch of 0.25m.
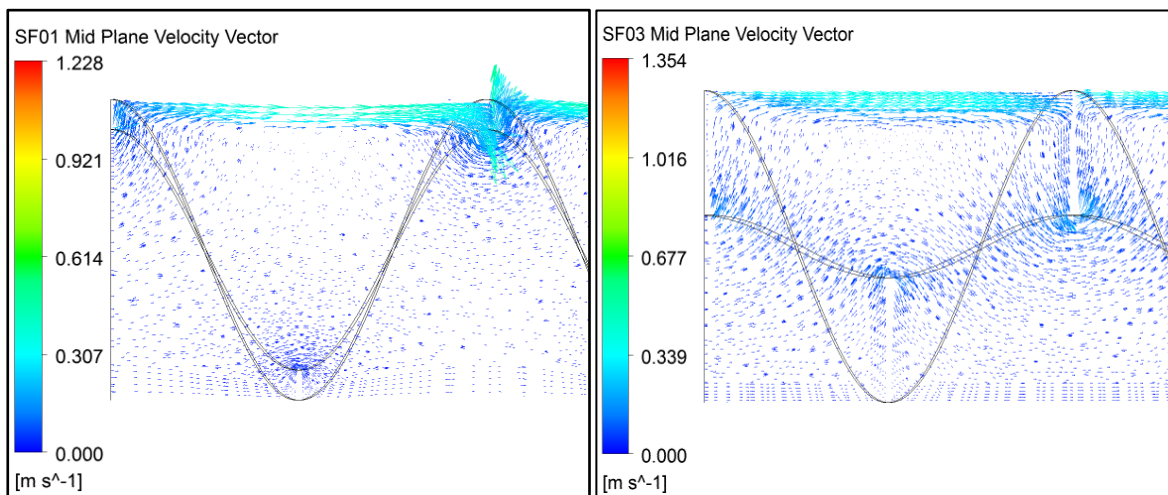

Figure 5.6.4: Velocity vectors for SF01 and SF03 showing of flow around baffle.

The flow in SF01 only has to travel under the baffle of 0.02m before flow can resume along the x-axis which does not require much energy. The flow around the baffle in SF03 has to travel under a baffle that is 0.08m in height which will obviously take more energy to achieve.

5.7   Optimisation of Results

The discussion of optimisation will start with a discussion of the various results that will be used. The pressure drop across the filter is one of the more important results that will be used. The residence time data will also be looked at for its suitability in the optimisation of the spiral baffled filters.

The results of the pressure drop and the power calculation show a definite relationship between the baffle height, pitch and the pressure drop. The relationship however of the baffle height and the pitch is not such that a single optimal solution can be found. Instead the two variables can be changed in value to adjust the power required. The use of a performance chart is one way to optimise the selection of baffle height, pitch and power required.
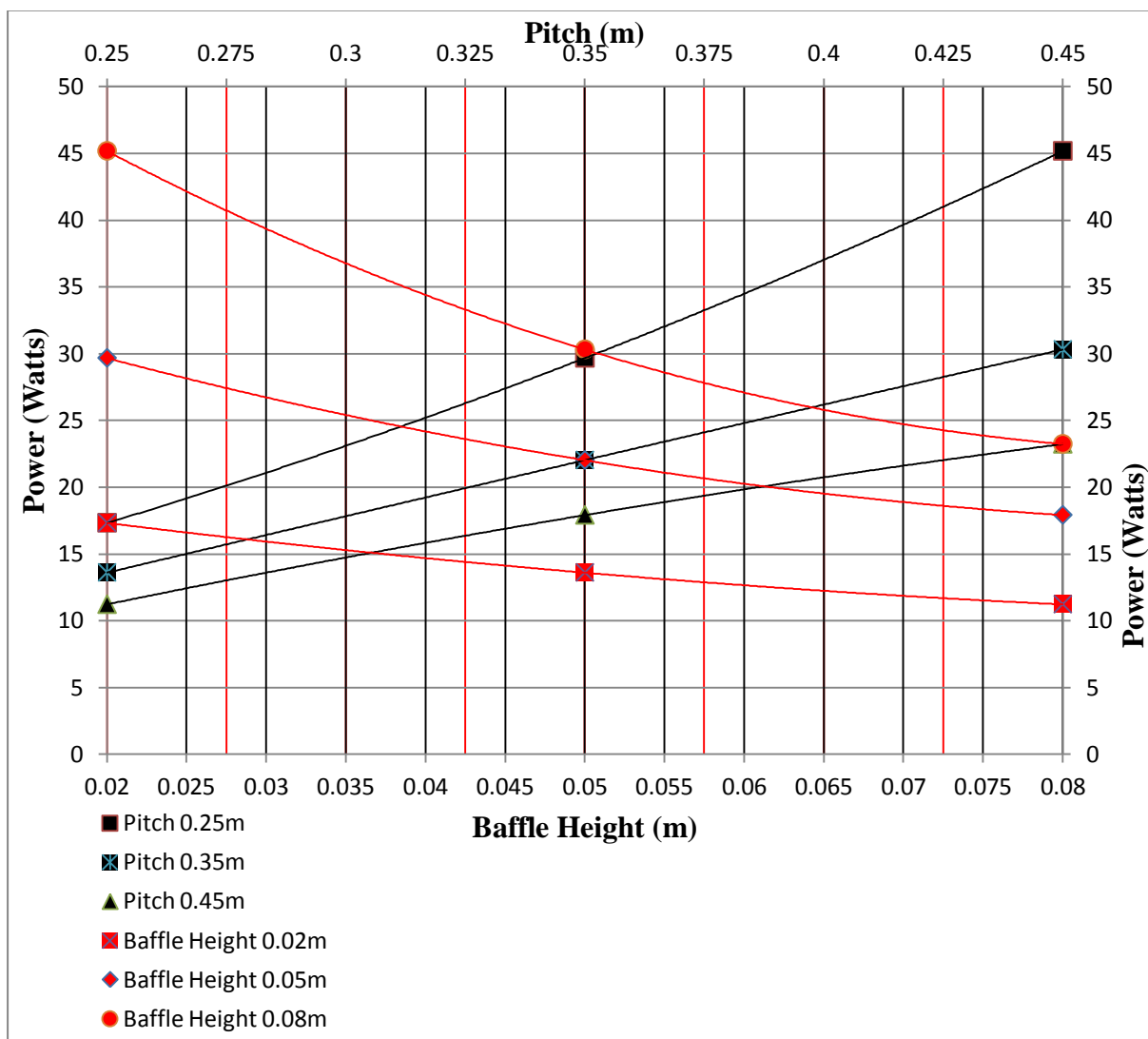

Figure 5.7.1: Performance chart for spiral baffle filters using pitch and baffle height.

The performance chart in figure 5.7.1 can be used to calculate the power required to drive the filter at various combinations of pitch and baffle height.

In this instance it is only valid within the following range:

- Pitch between 0.25m to 0.45m
- baffle height between 0.02m to 0.08m

The chart relies on results being interpolated between the points on the chart; the points have been fitted with a polynomial trend line of second order.

The equations for the trend lines are given below for various pitch where $h = baffle\ height$:

- Pitch 0.25m is $P = 1751.7h^2 + 288.98h + 10.84$
- Pitch 0.35m is $P = -74.537h^2 + 286h + 7.9093$
- Pitch 0.45m is $P = -761.04h^2 + 276.23 + 6.0012$

And trend line equations for various baffle height where $p = pitch$:

- Baffle height 0.02m is $P = 67.169p^2 - 77.515p + 32.501$
- Baffle height 0.05m is $P = 176.68p^2 - 182.47p + 64.244$
- Baffle height 0.08m is $P = 388.77p^2 - 381.84p + 116.33$

The performance chart has only been presented here as an example, interpolation between the various lines is at this point untested so data cannot be relied upon. The use of this type of performance chart is useful where several combinations of pitch and baffle height could be used to give the same power reading.

The use of residence time for optimisation is difficult in this case as the data shows no real correlation to the power or the baffle and pitch data. This could be due to error in the residence time calculations in Fluent™, or in the method used.

A plot of the power used for each filter and the corresponding residence time calculation is given in figure 5.7.2 on the next page. This plot does not reveal any particular pattern to the change in residence time with change in power.

Figure 5.7.2: Power change to residence time of each filter

Table 5.7.3 shows the data point used in figure 5.7.2., it has been sorted by increasing residence time.

Power	Pitch	Baffle Height	Model No.	Residence Time
17.9	0.45	0.05	SF08	69.5
23.2	0.45	0.08	SF09	93.3
11.2	0.45	0.02	SF07	95.7
22.0	0.35	0.05	SF05	140.5
30.3	0.35	0.08	SF06	142.0
13.6	0.35	0.02	SF04	198.3
17.3	0.25	0.02	SF01	264.3
29.7	0.25	0.05	SF02	411.7
45.2	0.25	0.08	SF03	498.6

Table 5.7.3: Power data sorted for increasing residence time

Looking at models SF08,9,7 and SF06,5,4 in table 5.8.5 the power appears to peak at baffle height of 0.08m and the residence time peaks at 0.02m. This can be seen in the bar chart on the following page (figure 5.7.4). This could indicate a trend but it is counter intuitive, as the residence time should increase as the power and resistance to flow increases. This increase in the resistance should correlate to an increase in the residence time.

This correlation between increased resistance and residence time can be seen with the first three models of pitch 0.25m, this is illustrated in the chart below.
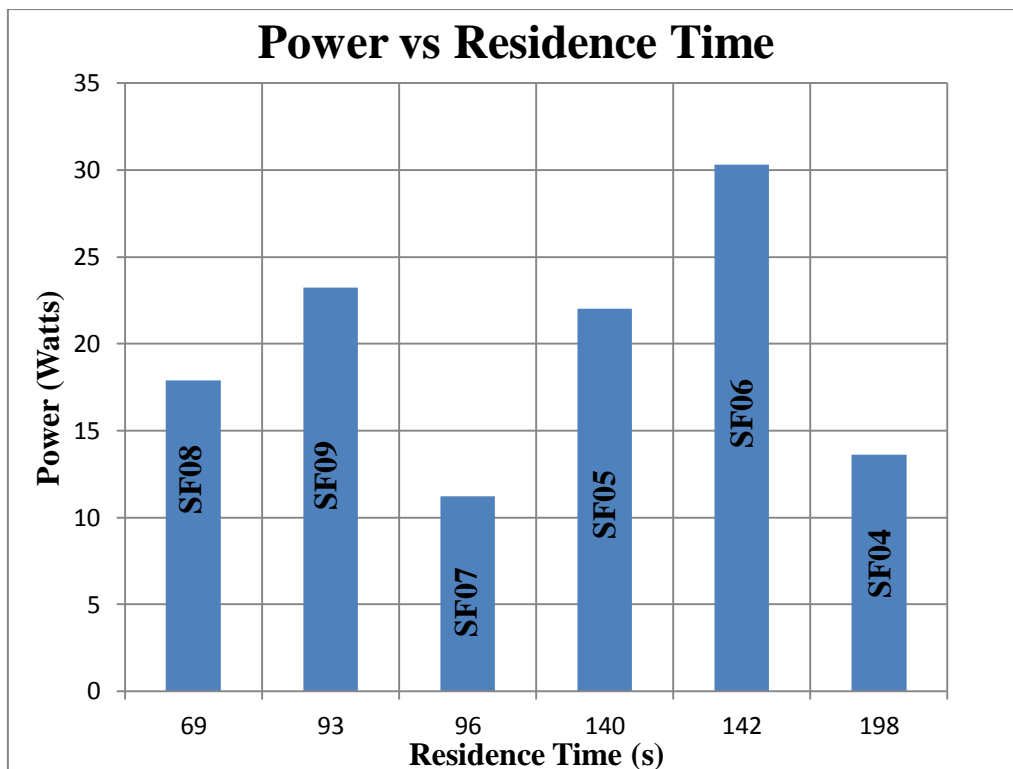
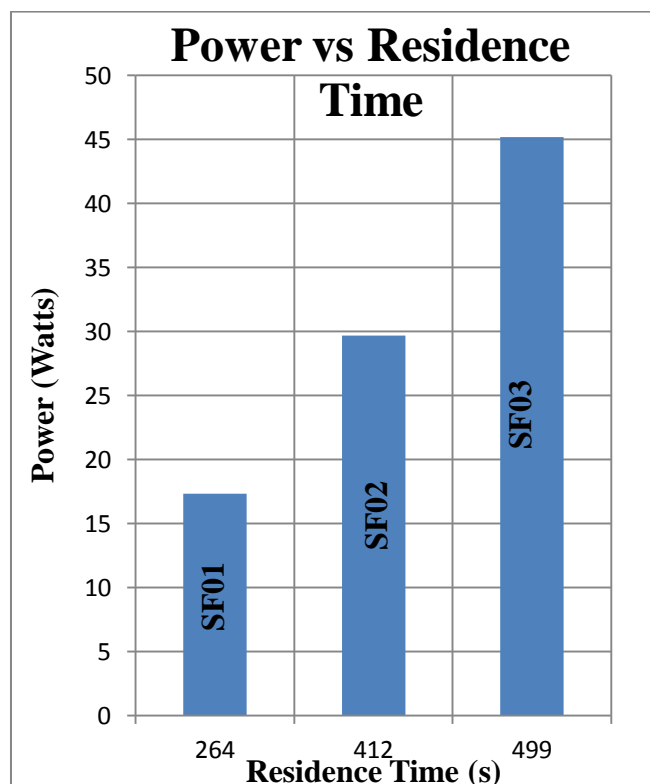**Figure 5.7.4:** Bar chart showing residence time of SF04-9 and corresponding power.

Figure 5.7.5: Bar chart showing residence time SF01-3 and corresponding power.

As can be seen from chart in figure 5.7.5 the power increases as the residence time increases. This is the result that would be predicted by considering the resistance to flow, more work will be required to establish the exact nature of the residence time change.

If the residence time does indeed increase as the power increases then the task of optimising the flow for residence time and power becomes difficult. The most realistic way to optimise the flow in regards to these two parameters is to optimise the power around a set residence time.

The residence time that is desired would need to be calculated based on the efficiency of the filter. The efficiency of the filter would need to be calculated from experimental testing of the filter. The performance of a filter is usually given the concentration of particulate upstream to the concentration of particulate downstream of the filter. The formula is given as:

$$Percentage\ Efficiency = \left(1 - \frac{C_d}{C_u}\right) \times 100$$

- $C_d = Downstream\ Concentration$
- $C_u = Upstream\ Concentration$

The results for residence time, when compared to the power input, do not give any confidence in their accuracy. Therefore the optimisation of the spiral baffle filters will have to be limited to the selection of pitch and baffle height to affect the power required.

5.8   Conclusion

The flow velocities through the water channel, along the x-axis, of all the spiral baffle models show a marked drop over the filter without the baffle SF10. The baffled models all show an increase in y-axis and z-axis velocities over SF10 indicating a tendency to push water out of the channel.

The baffle velocities showed the same pattern of behaviour for all filter models. The flow pattern, as projected onto longitudinal mid-plane, is downward, under the baffle then upward towards the water channel. As the baffle height is increased, it will force the flow to travel downward at a greater distance into the denser porous media. This flow pattern should provide better filtration than that of a horizontal filter without a baffle.

The CFD results for the sand filters show a definite correlation between the pitch, baffle height and the pressure drop. This relationship can be easily explained in terms of changing resistance to flow. As the pitch increases the resistance to flow decreases which correlates to a lower pressure drop. The inverse occurs with the baffle height, as the baffle height increases the resistance to flow increases and the pressure drop increases.

The relationship between pitch and baffle height allows the adjustment of pressure drop and therefore power input. The residence time data of the filters shows some strange behaviour;

the first three filters, of 0.25m pitch, show an increasing residence time with baffle height. This behaviour is expected if you consider the resistance to flow and the pressure drop data.

The remaining 6 filter models of 0.35m and 0.45m pitch show the inverse. The residence time decreased overall as the baffle height increased. There was a local minimum at baffle height of 0.05m in both the 0.35m and 0.45m pitch. This local minimum did not appear in filter model SF02 which has a baffle height 0.05m.

Two conclusions could be drawn from the data so far; the first conclusion is the data is in error. This may be attributed to the method of finding residence time or to the execution of the method by the author. The second conclusion is that the data shows a possible relationship that is hidden between the 0.25m and the 0.35m pitch. To be able to test this conclusion, as previously suggested, further analysis would be required.

Chapter 6 **MODEL VERIFICATION**

6.1   **Introduction**

Model verification is an important step in determining if a model accurately represents the intended conceptual description and solution of the model. The difficulty with verifying a CFD model is that no "proofs" exist for most of the complex problems solved with CFD (AIAA 1998). For this reason the verification process becomes iterative and ongoing until a reasonable result can be obtained.

Another issue with the verification process has to do with the issue of finding a correct answer. For this to be possible the CFD solution would need to be compared to either a benchmark case or experimental data (AIAA 1998). Unfortunately bench mark cases can only be found for the simplest of cases and experimental data is also subject to error and bias that will affect the result.

6.2   **Grid Convergence**

The establishment of grid convergence is one method that is used to give an indication of the accuracy of the results. The principle behind grid convergence is that the mesh size will be decreased, giving a finer mesh, until the solution does not change significantly. When grid convergence is established the solution is often referred to as being grid independent (Tu et al. 2008, p. 199).

It has been suggested that to test for grid independence or grid convergence the mesh sizes can be halved (Tu et al. 2008, p. 207). Therefore if the mesh sizes are given by $\Delta x, \Delta y$ and Δz then to test for grid independence the new mesh sizes will be $\Delta x/2$, $\Delta y/2$ and $\Delta z/2$. This method is difficult to employ with the academic licensed version of the ANSYS Fluent software due to the limitation on the number of nodes and elements.

Grid convergence to the standard set out above could not be achieved with these models due to the initial size of the mesh and the license limitations. In order to get the residual values to converge the mesh needed to be quite large to begin with, therefore halving the mesh size was not possible. Grid convergence was considered achieved when the mesh was made as fine as possible then the solution checked again to see the order of magnitude change.

6.3   **Iteration and Convergence Error**

Iteration error is suspected in the results of the residence time calculations. Iteration errors can be introduced if the iterative solution is ceased and restarted with a different time step. This is often done to speed up the overall solution process, it can however have an undesired effect with relation to the accuracy of the solution (Tu et al. 2008, pp. 200-6).

The results for residence time were calculated using a transient solver to allow the tracking of second phase volume fraction. The author varied the time step numerous times during the

calculation of the residence time. The only way to establish if the results are in error is to run the analysis again at a fixed time step and compare the solutions. Unfortunately due to time constraints and the length of time it takes to reach a solution at small time steps the author was unable to redo the calculations and check the solution.

6.4   **Summary**

The solutions obtained from this project may have errors that have been introduced through the manipulation of time step during the solution process. Grid independence over solution is considered to have occurred, however due to the node limit of the academic licence this has not been exhaustively tested.

Chapter 7 **FUTURE EFFORTS**

7.1   **Introduction**

Like most projects of this nature there are always areas that are identified as needing more research or further study. These areas will be highlighted here and some ideas on the future direction will be given.

7.2   **Model Validation**

Model validation is one of the most important areas of future work required. It was hoped that this could have been completed as part of this project but due to several constraints it has not. One of the major constraints to the validation of the numerical model is the creation of the physical model.

One of the best methods for the validation of the numerical model is by testing a physical model of the spiral baffled filter. The best way to physically model for flow testing is to construct a model from some transparent material. By using a transparent material the flow paths can be visualised with dye, it also allows for the visualisation of any turbulence that may occur around the baffles. However when the author looked into getting a modelled constructed it proved expensive to get a transparent model made.

It is hoped that validation of the numerical model will shed more light on the nature of the spiral baffle filter.

7.3   **Water Channelling Experiment**

It was identified earlier in section 3.5 on the methodology of modelling the water channel that several assumptions had been made. It would therefore be a worthwhile exercise to examine more closely the water channelling phenomena as it relates to the horizontal sand filter.

The behaviour of the interface between the low resistance zone and the high resistance sand at various velocities is needed. As can be seen from the results the velocities in the low resistance zone is up to three times as high as the average inlet velocities. These high velocities may well be enough to cause movement of the sand in this region.

7.4   **Alternate Spiral Geometries**

Many alternate spiral geometries remain that could be tested in a similar manner to those presented here. One such alternative is, to use threading terminology, the double start spiral baffle. The configuration of this baffle can be seen in figure 7.1 which shows two opposed spiral baffles traversing the length of the filter.
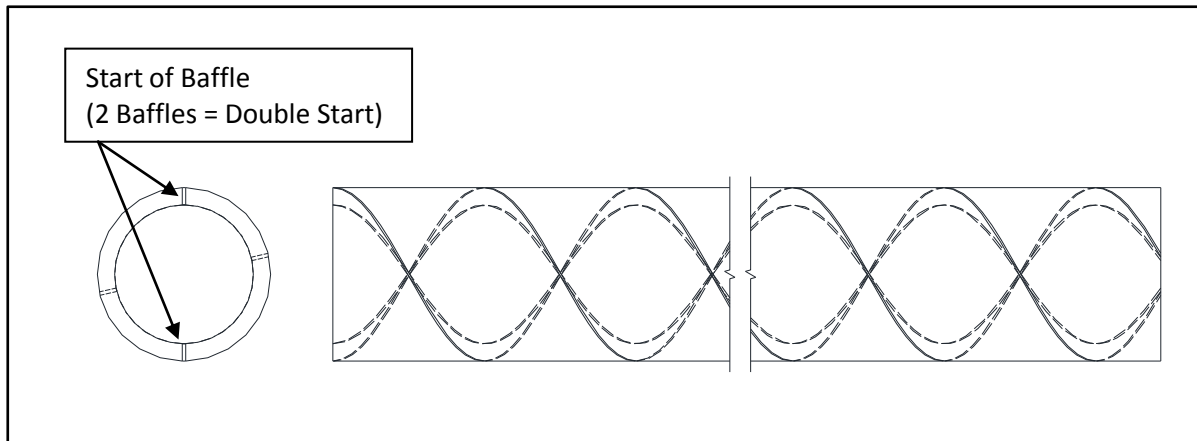
Figure 7.1: Double start spiral baffle filter.

7.5   **Modelling Filter Attachment Mechanisms**

The motivation behind modelling the attachment mechanisms within the filter is twofold. Firstly such a model would help to predict the behaviour of the spiral baffle filter as a filter. The model produced here simply models the flow behaviour, and whilst this is useful it does not allow for a prediction of the model as a filter.

Secondly, with a model of the filtration attachment mechanisms it would also be possible to model for the detachment of particles from the filter media. Modelling detachment would allow for studies to be made of the backwashing efficiency of the filter.

One possible way to model the behaviour of filter attachment is through the use of a multiphase model. Using this approach it may be possible to model the resistances at a macroscopic level over the filter domain.

7.6   **Summary**

More work is needed before the spiral baffle filter can become a commercially viable product. The modelling of filtration attachment in CFD is probably the most challenging area for further study. A successful CFD model of the attachment mechanisms of filtration would allow modelling for filtration efficiency and backwashing ability of the filter.

There are also many other possible spiral geometries that could be explored, with the double start configuration being just one. These could easily be modelled in the same way using CFD analysis and hopefully the results of physical validation.

The physical validation of the CFD simulation of spiral baffled filters is the next logical step for future work. If a suitable physical model could be created then experimental validation could prove very rewarding.

Chapter 8 **CONCLUSION**

8.1   **Introduction**

This dissertation looked at one possible solution to the need for economical treatment of drinking water. The solution looked at is the spiral baffled filter that is designed to be used in a horizontal configuration. This method of treatment was previously identified by Mossad & Aral (2010) as a solution to the phenomena of water channelling.

The aim of the dissertation was to study the flow through a horizontal spiral baffled sand filter focussing on the effect of changing baffle height and pitch. The residence time for fluid flow through the filter was also sort through the use of CFD analysis.

8.2   **Conclusions**

The various configurations of spiral baffle pitch and baffle height had a significant effect on the flow through the filter. The baffles were able to redirect the flow from the low resistance water channel back into the higher resistance porous zone. The result is the baffles cause an interruption in the water channel. This means that the high velocity flow path from inlet to outlet is no longer continuous.

The pitch of 0.25m gave the greatest resistance to flow and therefore had the greatest pressure drop. The baffle height of 0.08m had the greatest effect on flow along the x-axis (inlet to outlet) with the flow along the z-axis being greater. This meant that the baffle height of 0.08m had the greatest effect on the residence time.

The residence time results showed some unexpected results with the filter models of pitch 0.35m and 0.45m. The expected results were reflected in filter models SF01,2 and 3 which showed an increase in residence time as the baffle height increased. The reason for the unexpected results in the other filter models is not entirely known.

 It is suspected that the transient solution time step was altered too often during the calculation of the solution. The time step was altered to try and reduce solution time but may have had an adverse effect on the results.

8.3   **Recommendations**

One of the most important recommendations is in regards to the calculation of the residence time. The results from this analysis will need to be recalculated for two reasons; to check the accuracy of the results and to establish the reason for the unusual residence time results.

The analysis should include several values of pitch between 0.25m and 0.35m to try and identify if any unique behaviour in regards to residence time occurs. The residence time in general is a good method of establishing the time it takes for fluid flow to traverse the filter. It does not however give any indication of the filtration efficiency.

It is recommended also that the CFD model be adjusted to include a way of modelling the attachment of particles in the filter. In this way the analysis could be run again as a multiphase solution and the volume fraction of particulate in the filter could be tracked. This may give an indication to the possible filtration efficiency.

Finally the CFD models will need to be validated at some stage through the physical experimentation on a scale model. The information gathered from this exercise would be invaluable to the future research of the spiral baffled filter.

Appendix A - Project Specification

University of Southern Queensland
FACULTY OF ENGINEERING AND SURVEYING
ENG 4111/4112 Research Project
PROJECT SPECIFICATION

FOR:	Richard Ryan
STUDENT No:	0050009002
TOPIC:	NUMERICAL MODELLING OF HORIZONTAL FLOW IN A SAND FILTER
SUPERVISORS:	Ruth Mossad
ENROLMENT:	ENG4111 – S1, EXT, 2011 ENG4112 – S2, EXT, 2011
SPONSORSHIP:	Faculty of Engineering & Surveying University of Southern Queensland.
PROJECT AIM:	This project aims to use computational fluid dynamics software to model the flow of water through a horizontal laid sand filter fitted with a spiral baffle and to optimise the configuration of this baffle.

PROGRAMME:

1. Research into the use of sand filters and current limitations of using these filters in a horizontal configuration.

2. Develop skills in the use of CFD software for the modelling fluid flows.

3. Develop a CFD model of the spiral baffled filter to look at the effects of water channelling in the system.

4. Determine the optimal configuration of a spiral baffle to give the greatest retention time at the lowest power input by investigating various configurations of baffle height and pitch.

As time permits:

5. Validate the CFD model with experiments on a physical spiral baffled filter.

6. Investigate ways to compare the effectiveness of horizontal and vertical sand filters.

AGREED_____(Student)	_____Approved_____(Supervisor)
DATE: 22/03/2011	DATE: 22/03/2011
Assistant Examiner: _____	

Appendix B - Supplimentary Results

The supplemenatry results have been provide here to present velocity vectors and pressure contours for each spiral filter. In addition to this the velocity plots at the baffle have also been provided for each filter. A short description of each has also been provided to aid interpretation of the plots.

Results SF01

Velocity vectors below are given either projected onto the longitudinal mid-plane or in the case of the top view vectors are of the entire bulk. The filter model SF01 has a pitch of 0.25m and a baffle height of 0.02m.
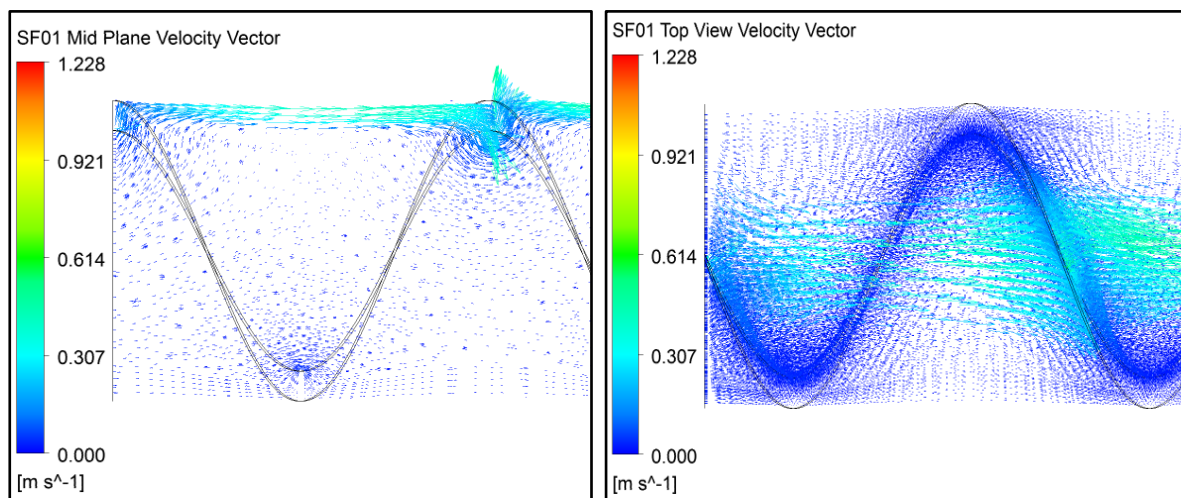
Figure B.1: Velocity vectors mid plane and top view of spiral baffled filter SF01.

The velocity vectors at the mid-plane show the flow path as it travels downward and under the baffle. Once passed the filter it rises towards the water channel again.

The velocity projected onto a line on the baffle mid-plane shows a marked velocity in the negative direction along the z-axis (figure B.2). This indicates a flow that is in the opposite direction to the rotation of the spiral.
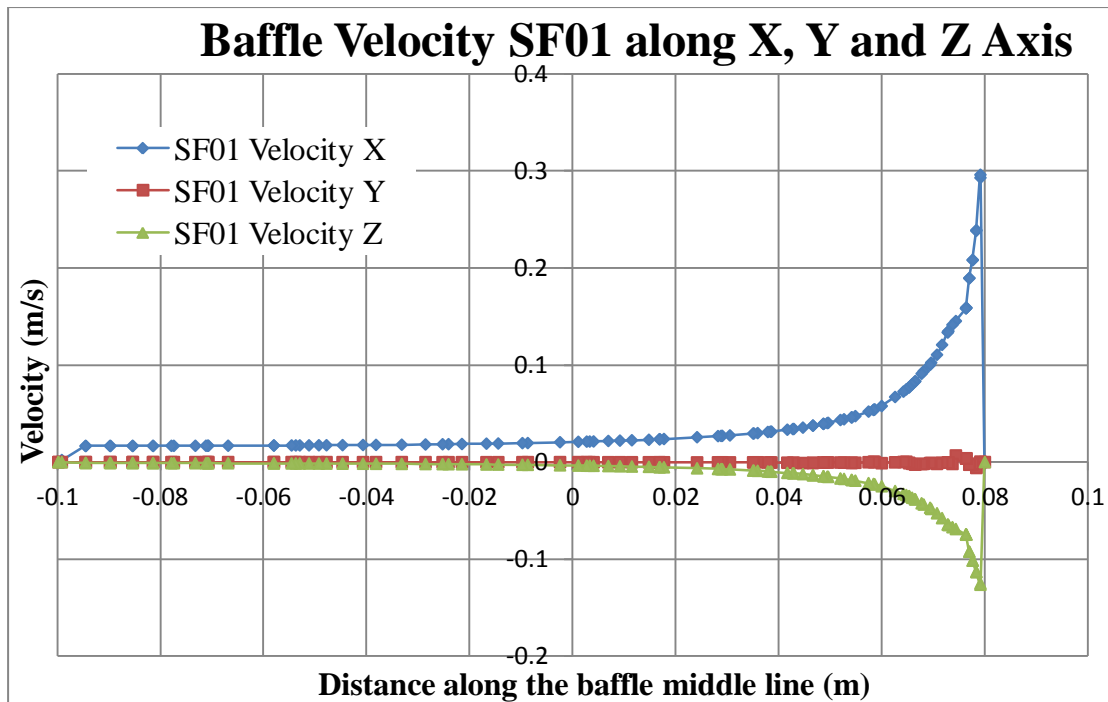
Figure B.2: Baffle velocity along x, y and z-axis at baffle mid line SF01.

The pressure drop given in figure B.3 has been projected onto the longitudinal mid-plane of the filter. The contours show a gradual drop in pressure across the length of the filter, decreasing to zero gauge pressure at the outlet.
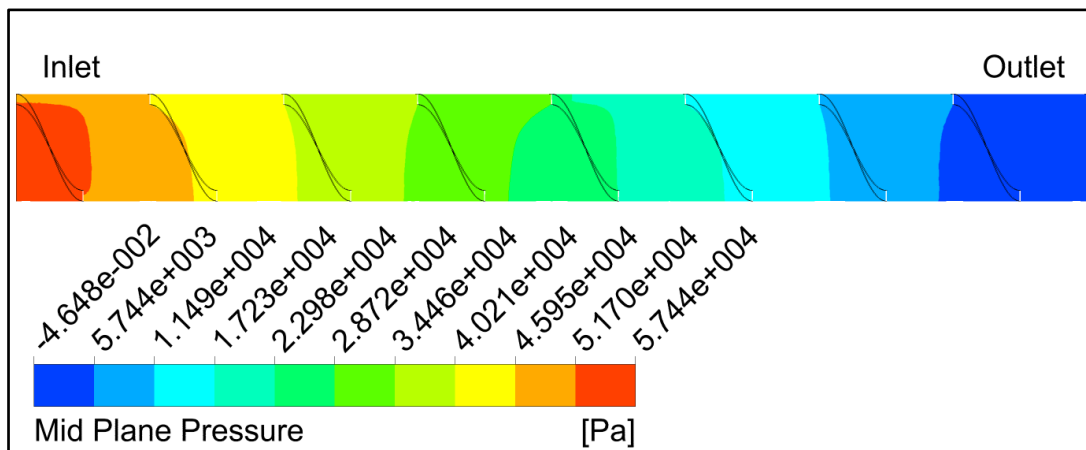
Figure B.3: Pressure drop along mid plane of filter SF01.

Results SF02

The results for SF02 which has a baffle height of 0.05m and a pitch of 0.25m. Velocity vectors given in figures B.4 and B.5.
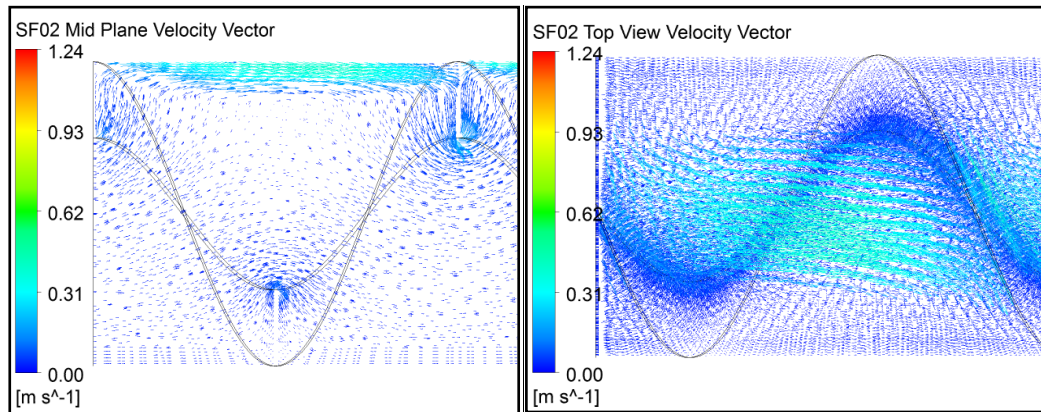
Figure B.4: Velocity vectors mid plane and top view of spiral baffled filter SF02.
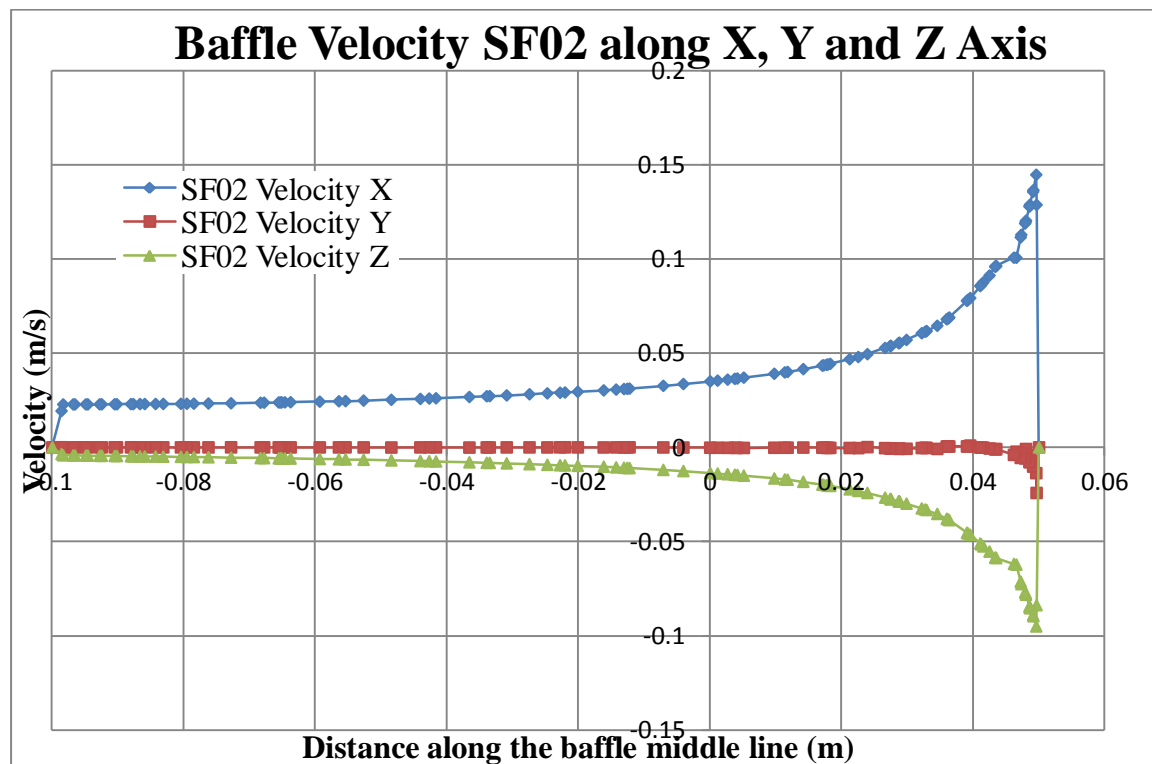
Figure B.5: Baffle velocity along x, y and z-axis at baffle mid line SF02.
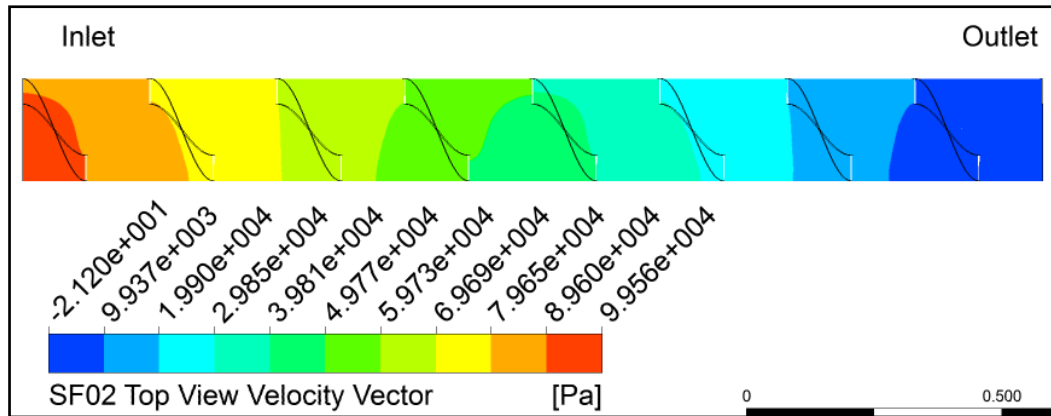
Figure B.6: Pressure drop along mid plane of filter SF02.

Results SF03

Results for filter model SF03 which has a baffle height of 0.08m and a pitch of 0.25m. The baffle height here is the greatest at 0.08m for the 0.25m pitch. As can be seen in figure B.7 the flow has to travel much further downward (negative y-axis) that the previous two models of 0.05m and 0.08m.
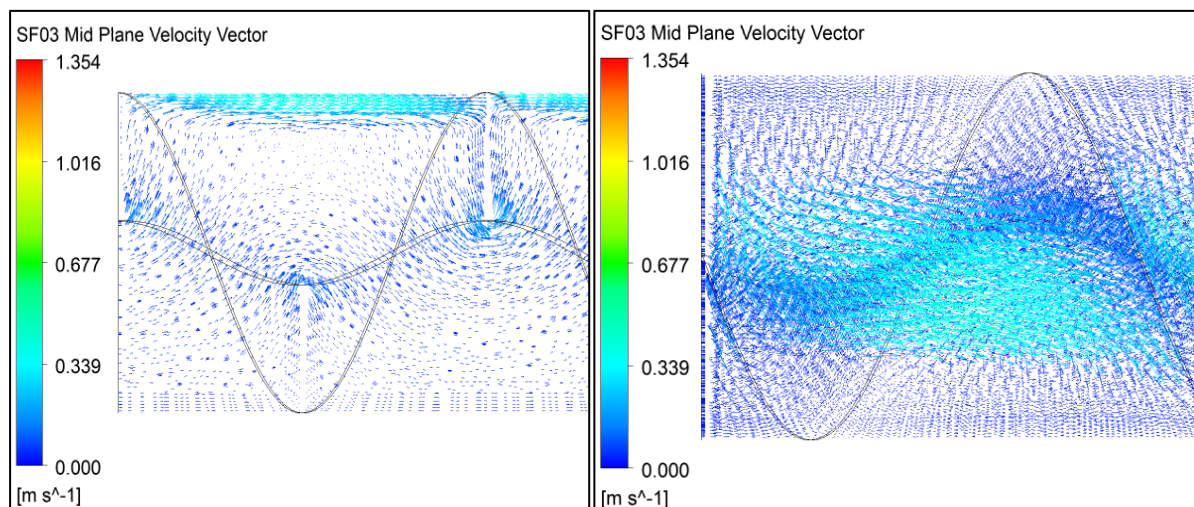
Figure B.7: Velocity vectors along the mid plane and top view of spiral baffled filter SF03.
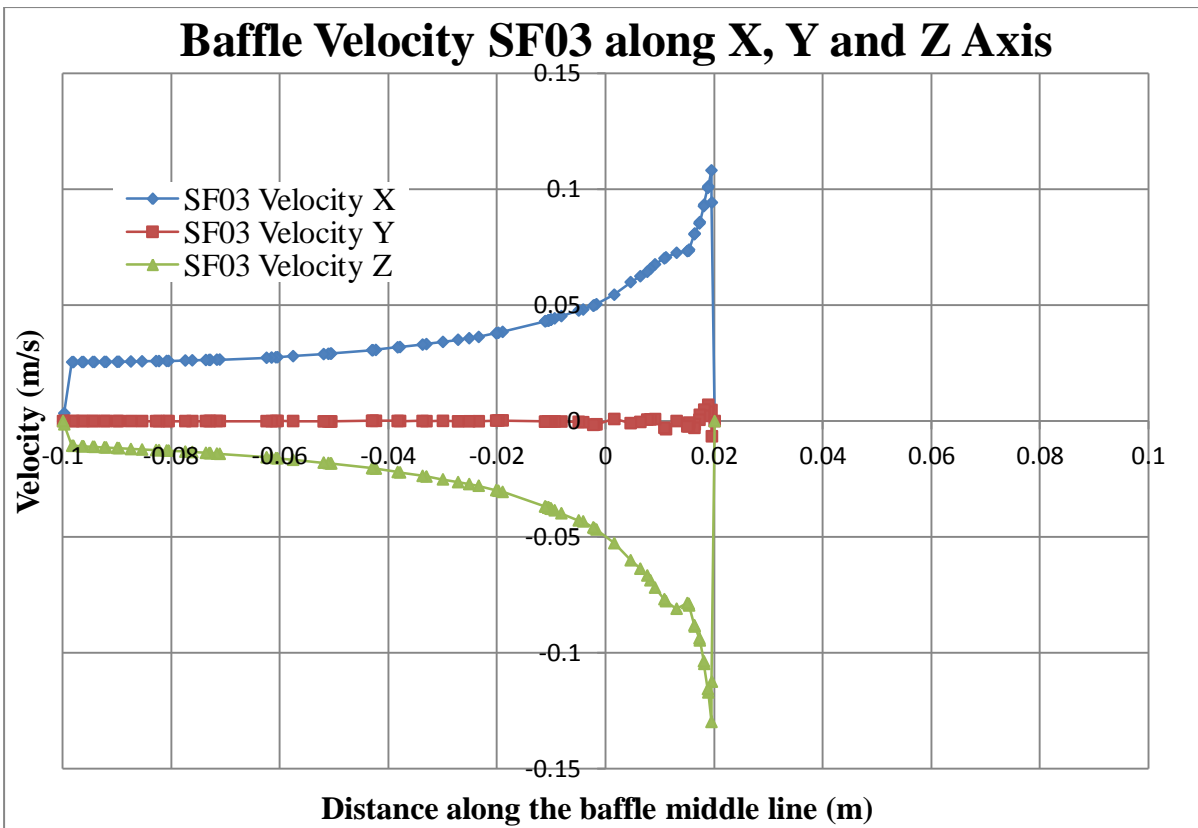
Figure B.8: Baffle velocity along x, y and z-axis at baffle mid line SF03.

Velocity plot given in figure B.8 show a larger z-axis magnitude than the x-axis. This indicates a greater flow in the reverse direction to spiral rotation, this can be attributed to the increased pressure drop (figure B.9).
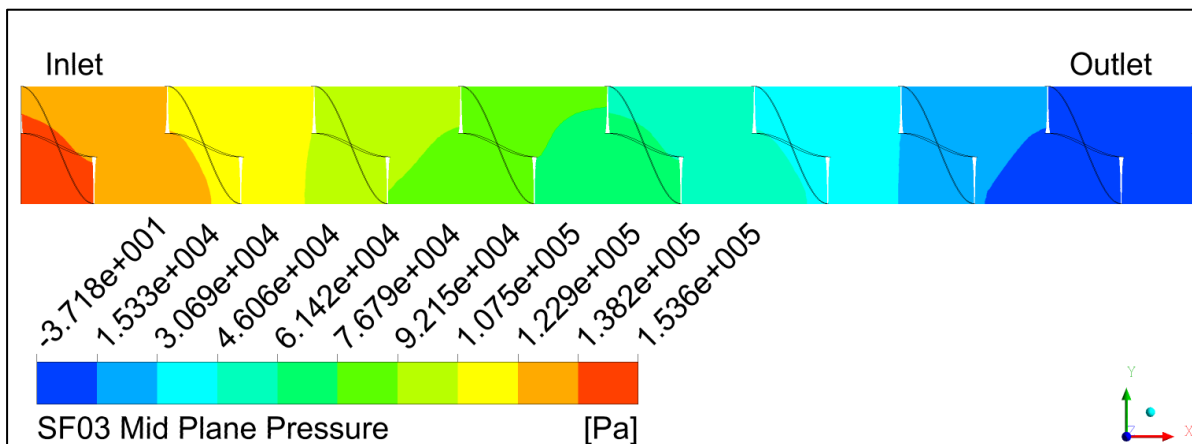
Figure B.9: Pressure drop along mid plane of filter SF03.

Results SF04

The velocity vectors along the mid plane of the filter show the same pattern of flow under the baffle as the other models (figure B.10). The baffle is 0.02m in height and the pitch is 0.35m for model SF04.
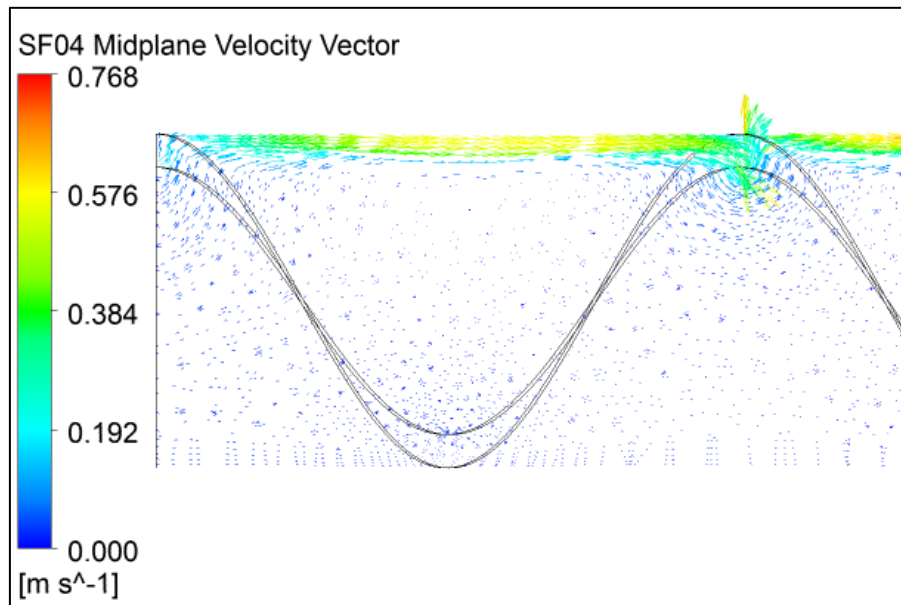
Figure B.10: Velocity vectors along the mid plane of spiral baffled filter.
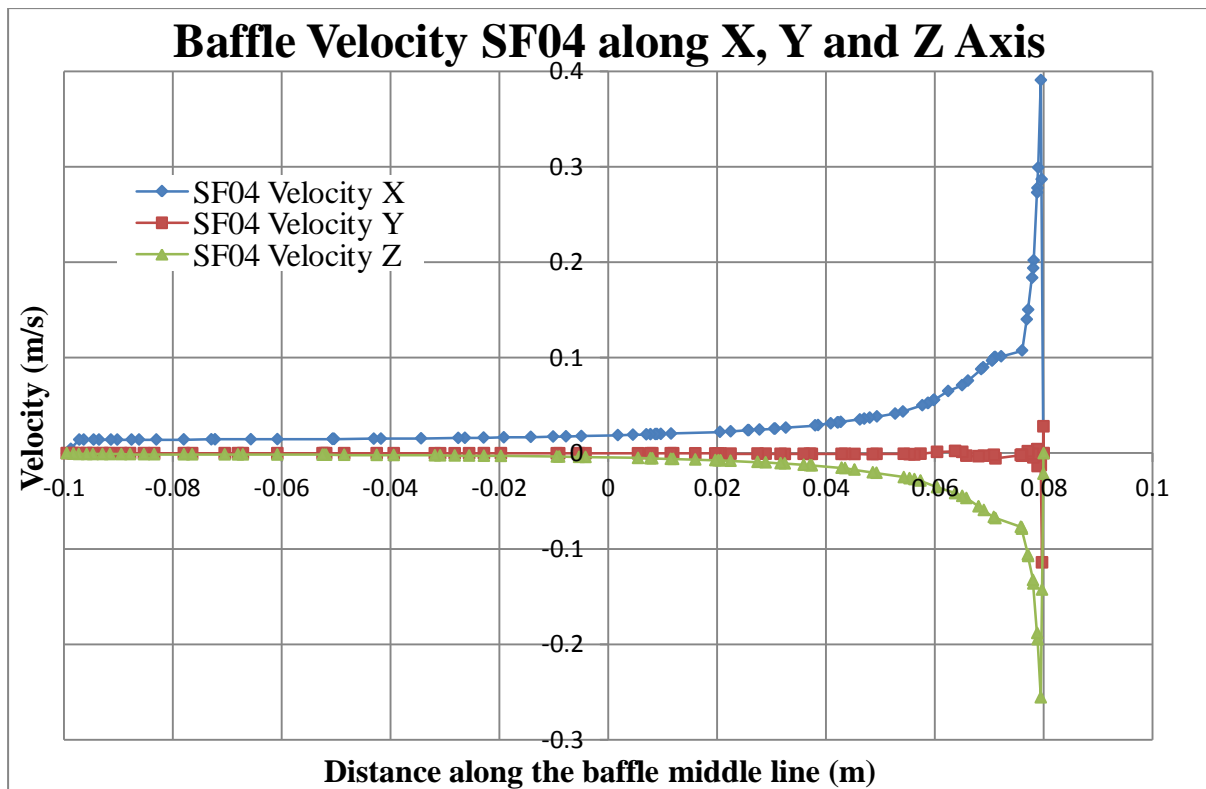
Figure B.11: Baffle velocity along x, y and z-axis at baffle mid line SF04.

Velocity along the x-axis is greatest for SF04 (figure B.11) with the z-axis showing the negative flow in the reverse direction to spiral rotation. Figure b.12 shows the pressure drop across the filter body for SF04.
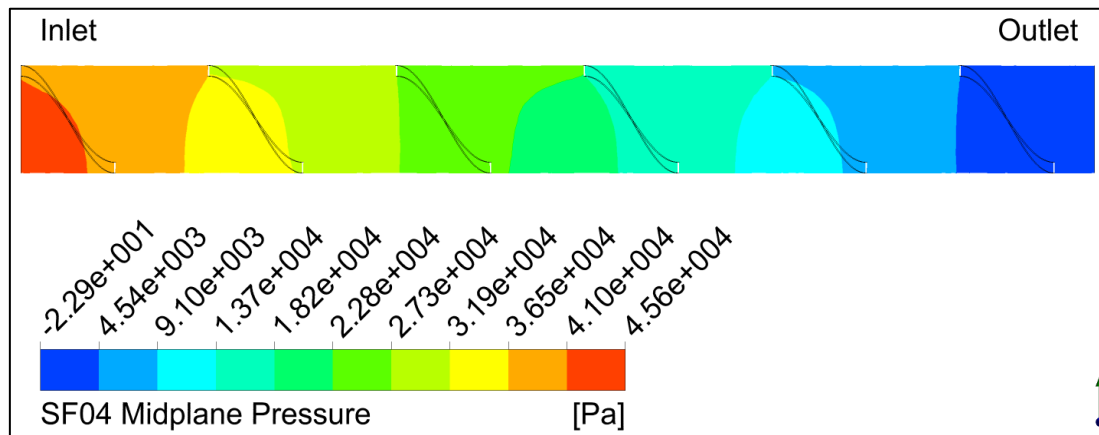
Figure B.12: Pressure drop contours across the filter.

Results SF05

The velocity vectors along the mid plane of filter SF05, having a pitch of 0.35m and a baffle height of 0.05m, are presented below. The flow shows the same characteristics as that of SF04 with the 0.02m baffle height. The water channel has the highest velocity which then slows as it reaches the baffle. At that point it travels down under the baffle then up the other side (figure B.13).
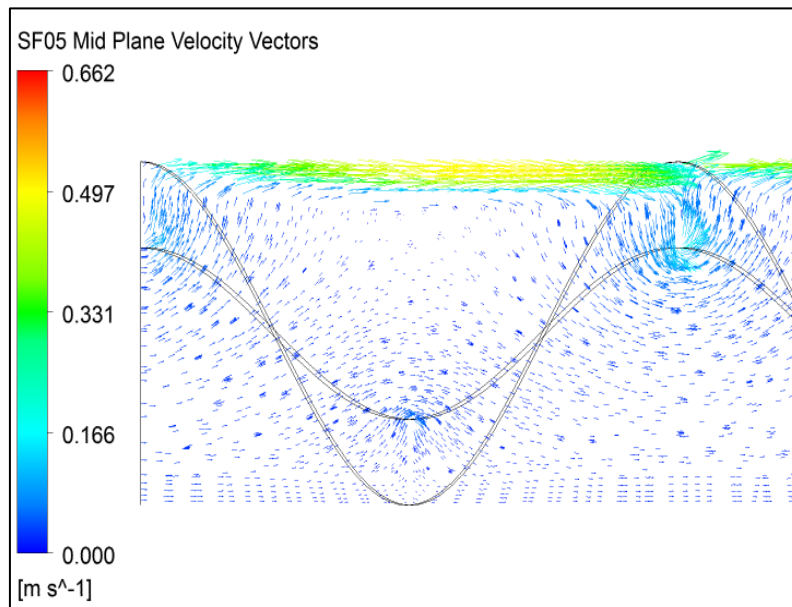
Figure B.13: Velocity vectors along the mid plane of spiral baffled filter SF05.

The components of velocity at a line vertically through the baffle are presented in figure B.14 below. The velocity components vary from that of the smaller baffle height with the x-axis

component and z-axis component being almost opposite in magnitude at the base of the baffle. The x-axis component has a peak value of 0.12m/s just under the baffle, the velocity then drops due to zero velocity at the baffle boundary. The z-axis behaves in a similar way with a peak velocity of -0.115m/s, with the negative magnitude again this signifies flow in the opposite direction of spiral at a point just below the baffle.
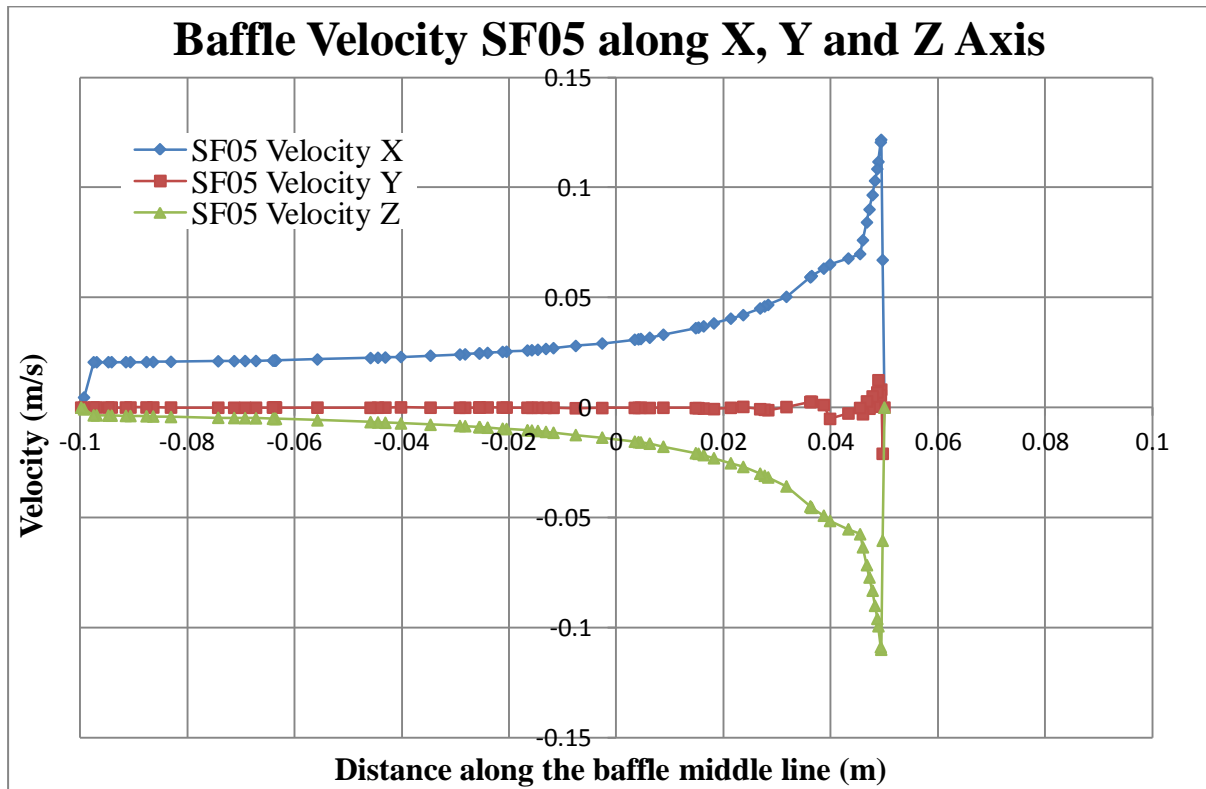
Figure B.14: Baffle velocity along x, y and z-axis at baffle mid line SF05.

The pressure contours shown in figure B.15 indicate the drop in pressure across the length on the mid-plane.
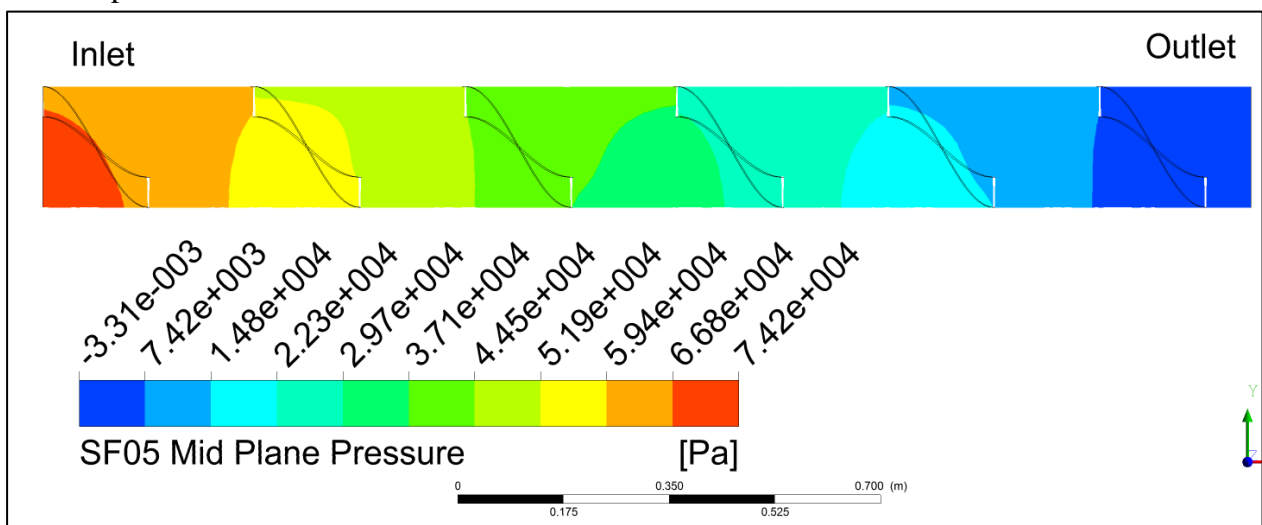
Figure B.15: Pressure contours along the mid plane of spiral baffled filter SF05.

Results SF06

The results from model SF06 which has a baffle height of 0.08m and a pitch of 0.35m will now be presented. The velocity vectors, given in figures 5.7.1 and 5.7.2, give a good visual indication of the flow paths in and around the baffle. As with the previous models SF04 and SF05 the flow as viewed from the mid-plane travels down and around the baffle. The high velocity zone as expected is in the water channel with the velocity slowing towards the baffle.
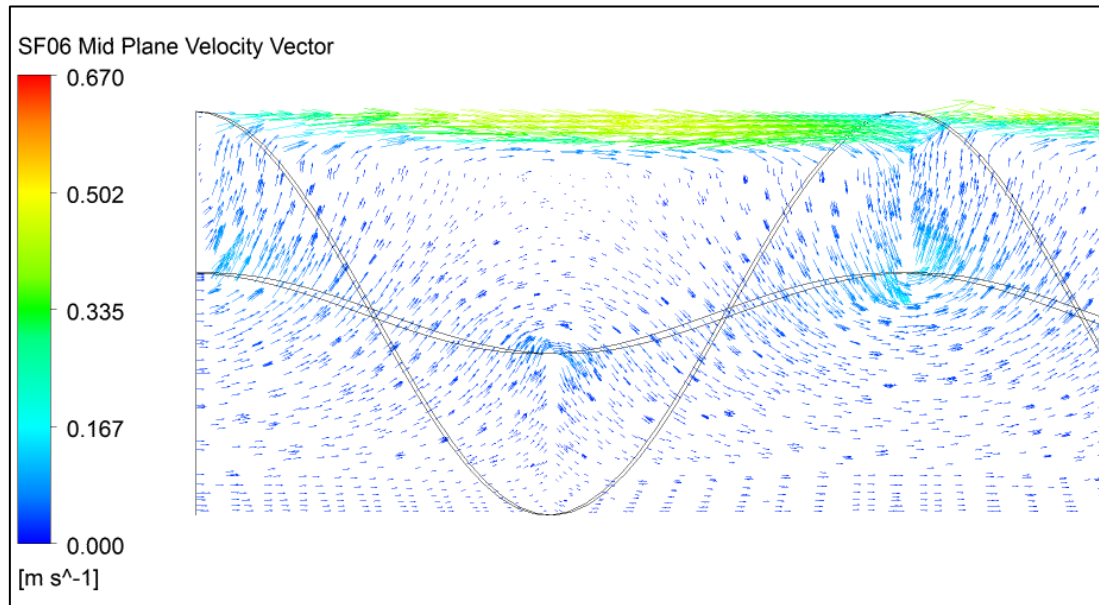
Figure B.16: Velocity vectors along the mid plane of spiral baffled filter SF06.

Velocity along the line passing vertically through the baffle of SF06 is presented in figure B.17 below. As the baffle height in this case is 0.08m in height the point at which the velocity stops is at a distance that corresponds to the base of the filter. Velocity along the z-axis is the greatest in this case at a value of -0.135m/s which is an indication of the flow going in the opposite path of the spiral baffle.
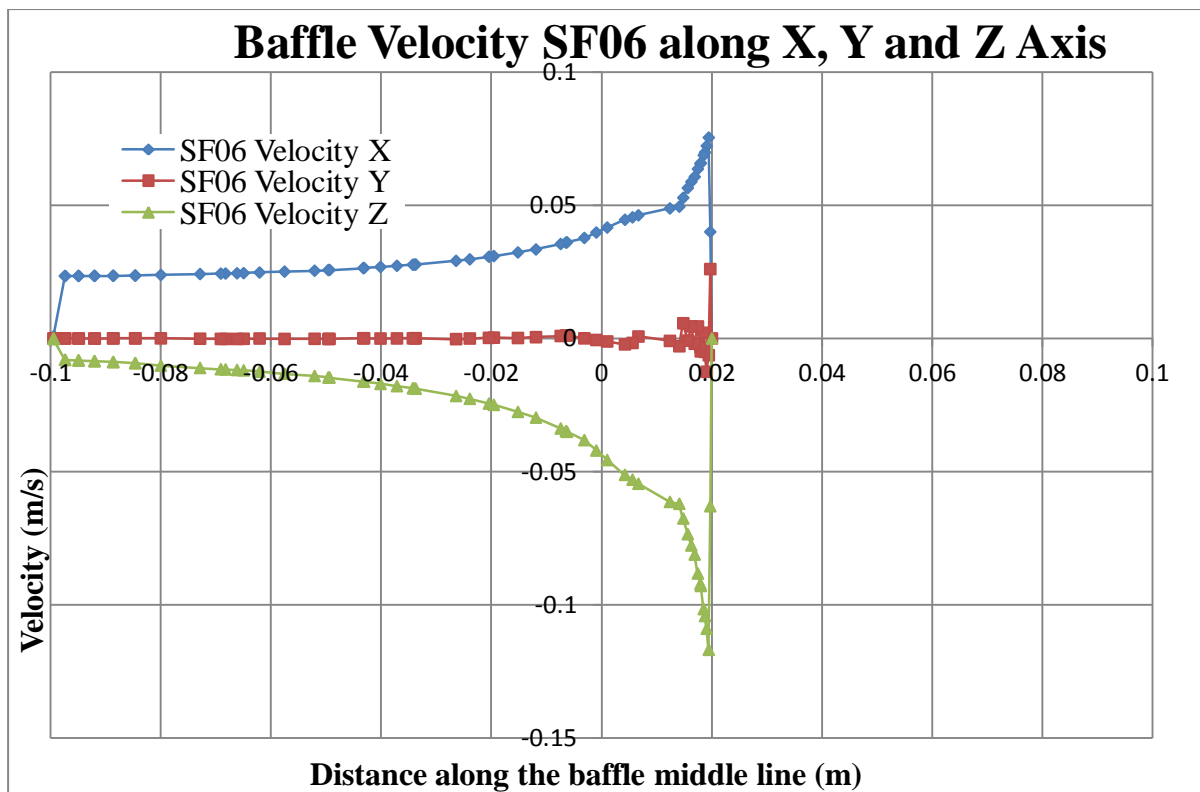
Figure B.17: Baffle velocity along x, y and z-axis at baffle mid line SF06.

The high velocity in the negative direction (figure B.17) along the z-axis is due to the increased pressure drop experienced in filter model SF06 (figure B.18).
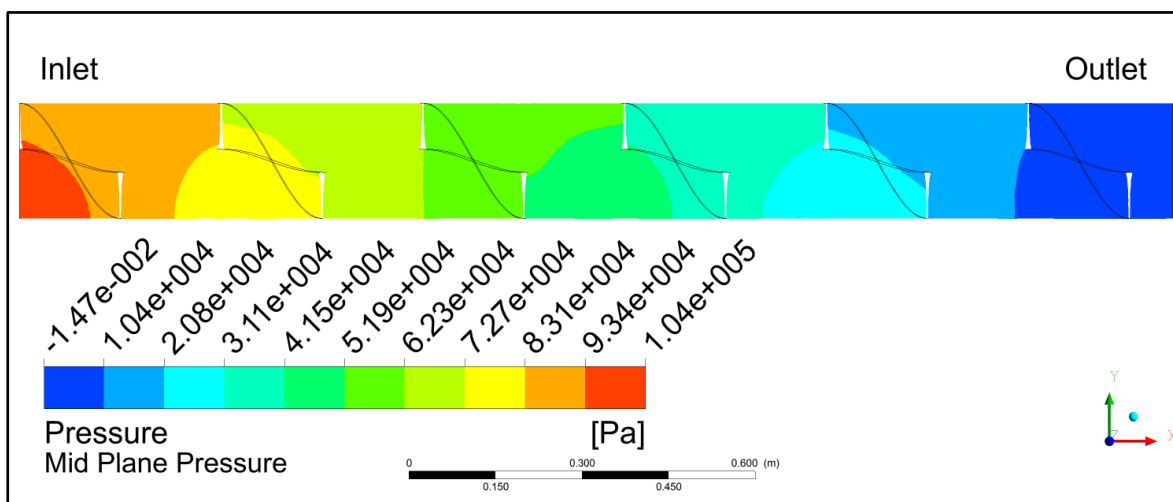

Figure B.18: Pressure drop along the mid plane of model SF06.

Results SF07

The results for the filter model SF07 are presented below; this model has 0.45m pitch and a baffle height of 0.02m. The velocity vectors show a very high flow rate in the water channel zone with some slowing of velocity before the baffle. The flow again passes downward and under the baffle wall in a similar pattern to the other filter models.
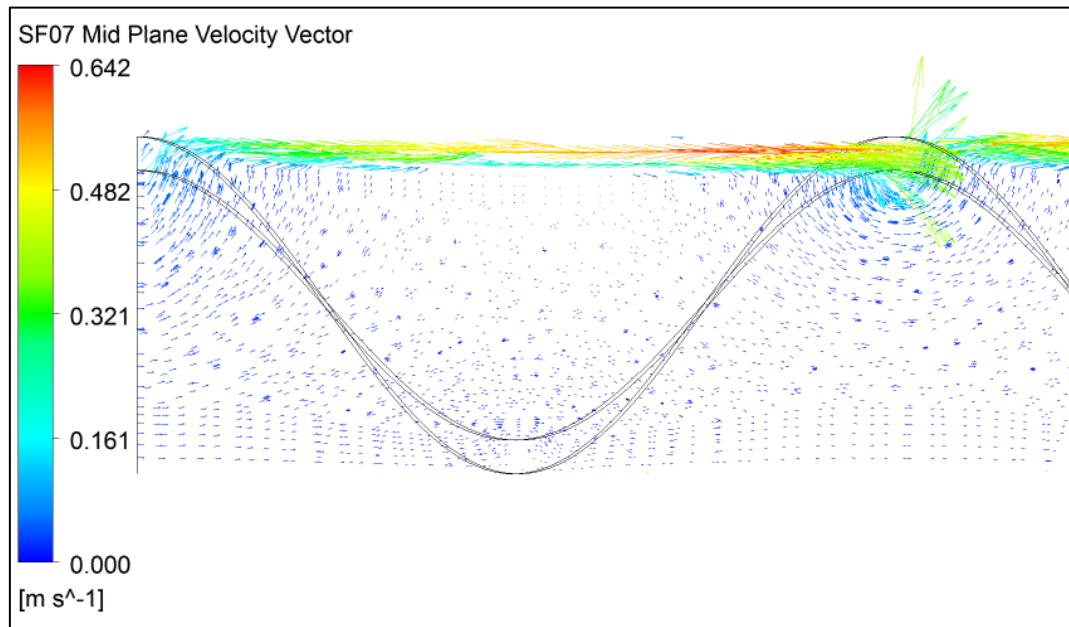
Figure B.19: Velocity vectors along the mid plane of spiral baffled filter SF07.

When the velocity at a vertical plane through the baffle are graphed (figure B.20) it confirms the high velocities. The x-axis velocity is just below 0.25m/s at the point just below the baffle wall. The z-axis velocity again shows a high velocity flow in the opposite direction to the turn of the baffle. And the y-axis velocity shows some up and down flow of modest velocity just below baffle wall.
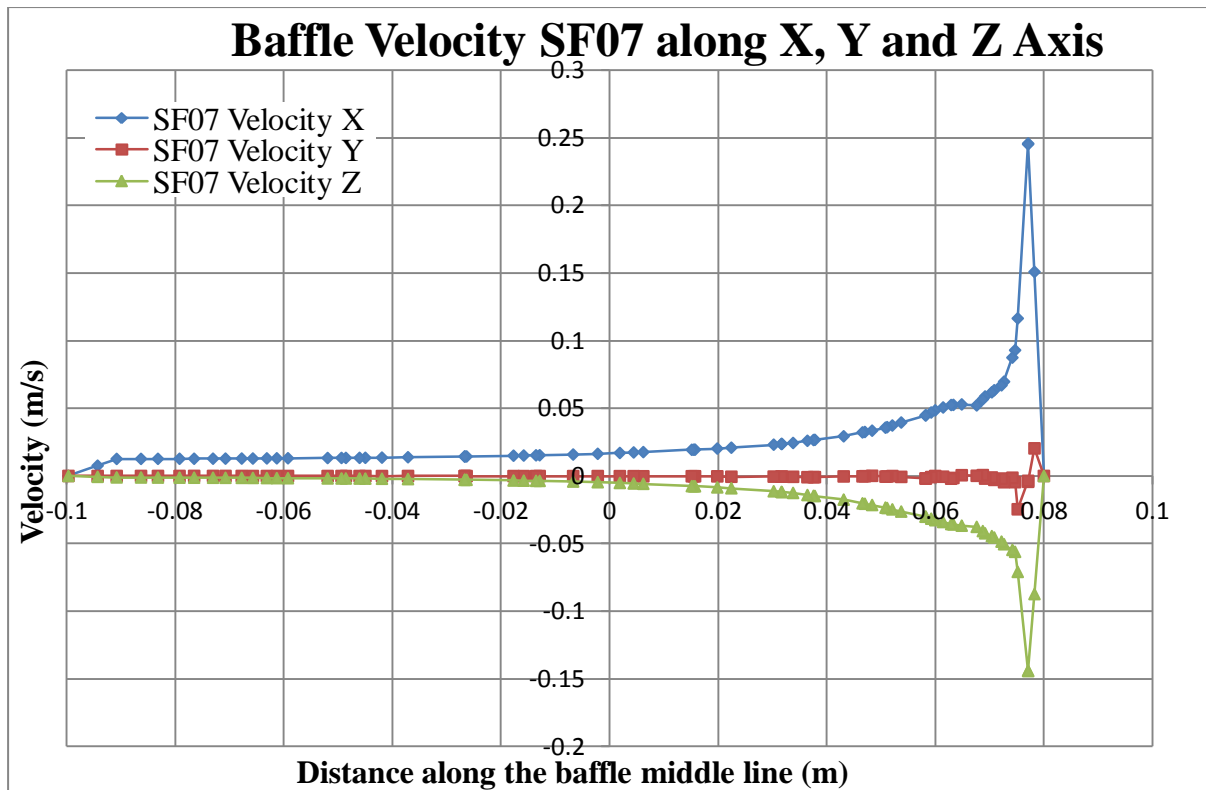
Figure B.20: Baffle velocity along x, y and z-axis at baffle mid line SF07.

Lower z-axis velocity (figure B.20) in SF07 correlate to the lower pressure drop experienced in this filter model (figure B.21).
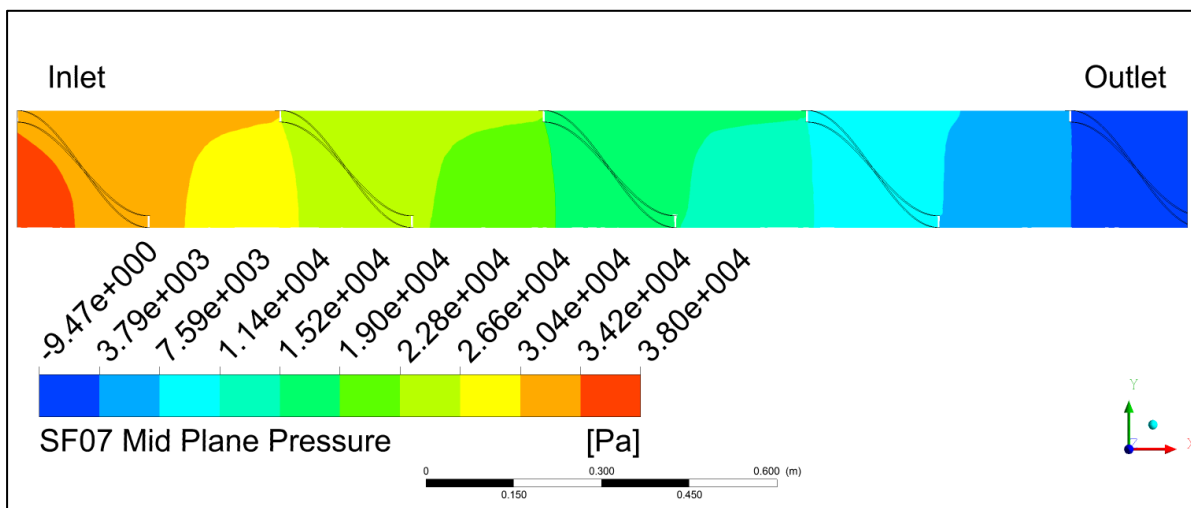

Figure B.21: Pressure drop along the mid plane of model SF07.

SF08 Results

The velocity vectors in figure B.22 show much higher velocity in the channel section. This model has a pitch of 0.45m and a baffle height of 0.05m. The flow shows the same downward behaviour exhibited by the other models.
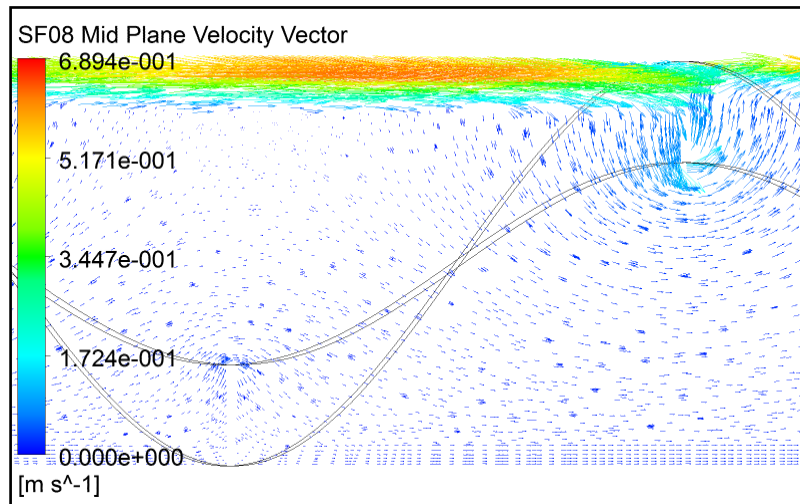

Figure B.22: Velocity vectors along the mid plane of spiral baffled filter SF08.

Velocity when plotted (figure B.23) shows an almost equal absolute magnitude along the x-axis and z-axis. This is similar to other models of different pitch but with the same baffle height of 0.05m.
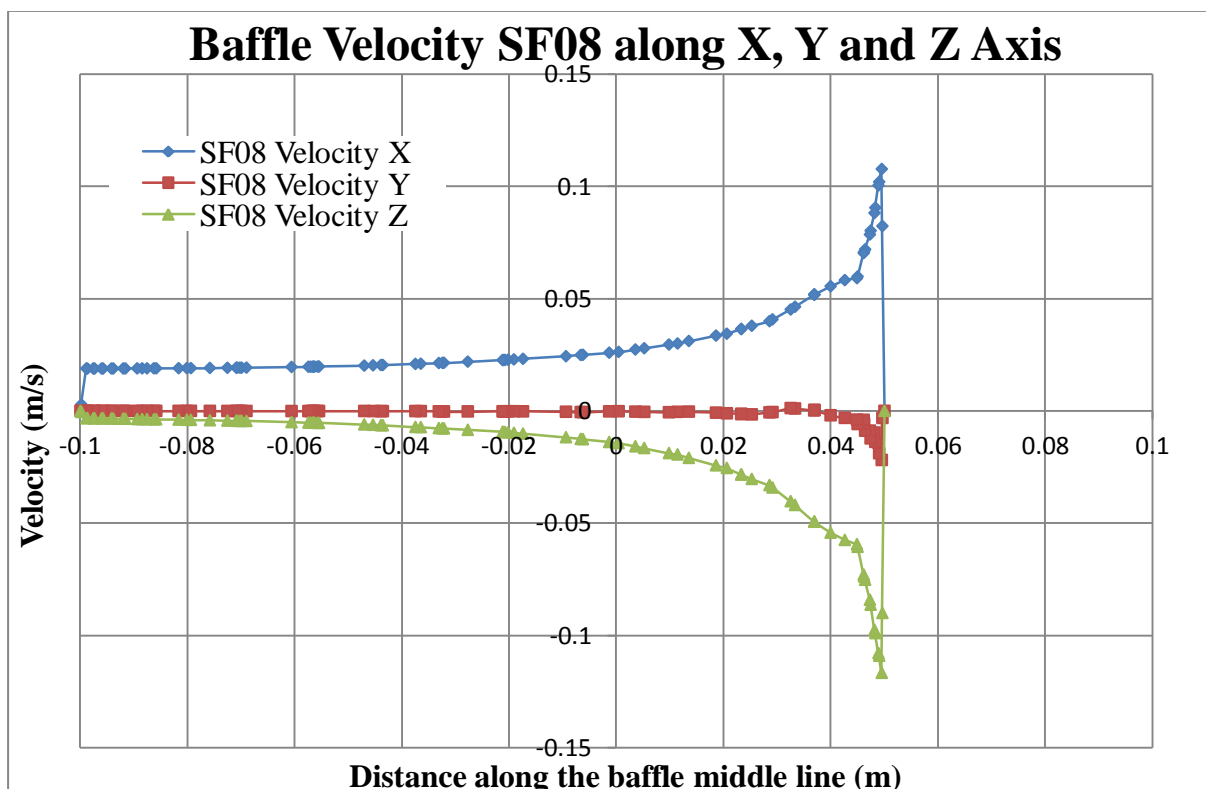

Figure B.23: Baffle velocity along x, y and z-axis at baffle mid line SF08.

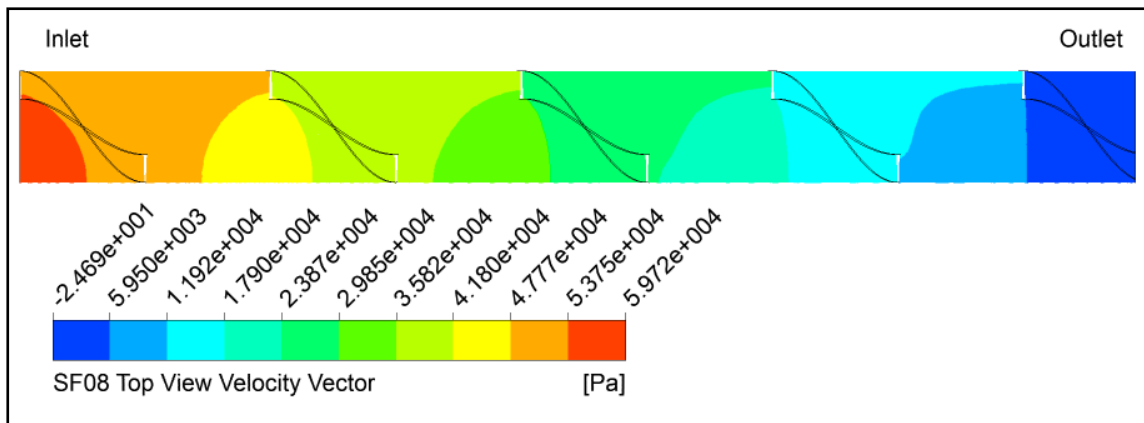The pressure drop across the filter model Sf08 can be seen in figure B.24 below.

Figure B.24: Pressure drop along the mid plane of model SF08.

Results SF09

The velocity vectors for SF09 are shown in figure B.25 below, as with SF08 and SF07 the velocity in the channel sect is high. All three filter models share the same pitch at 0.45m and SF09 has a baffle height of 0.08m.
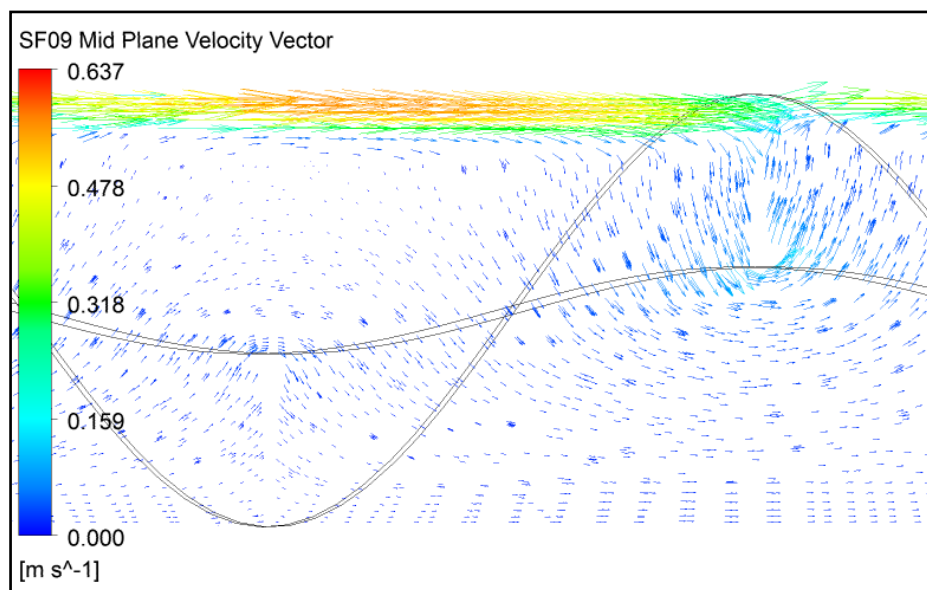

Figure B.25: Velocity vectors along the mid plane of spiral baffled filter SF09.

The velocity plots show the same pattern shared amongst filters of 0.08m baffle height, that is high z-axis velocity. The z-axis velocity is greater than that along the x-axis, again this is due to the pressure drop.
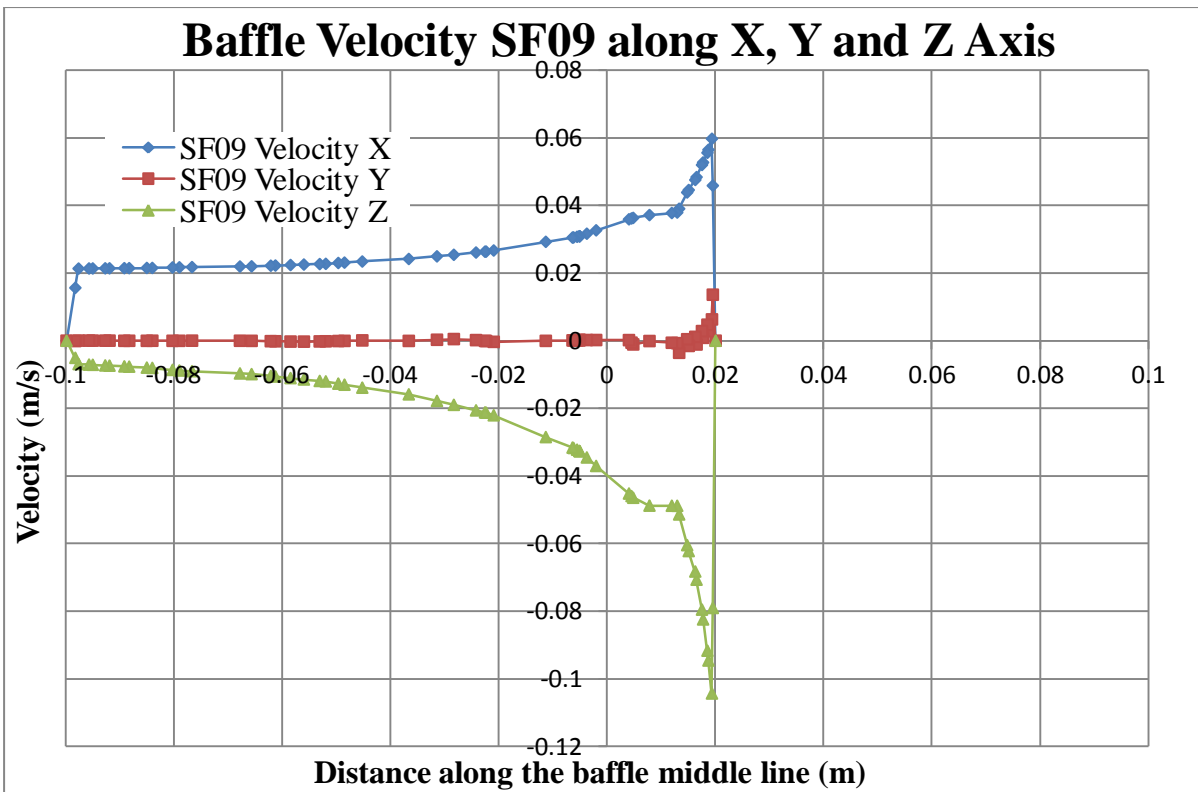
Figure B.26: Baffle velocity along x, y and z-axis at baffle mid line SF09.

Figure B.27 shows the pressure drop across the spiral baffled filter SF09 from inlet to outlet.
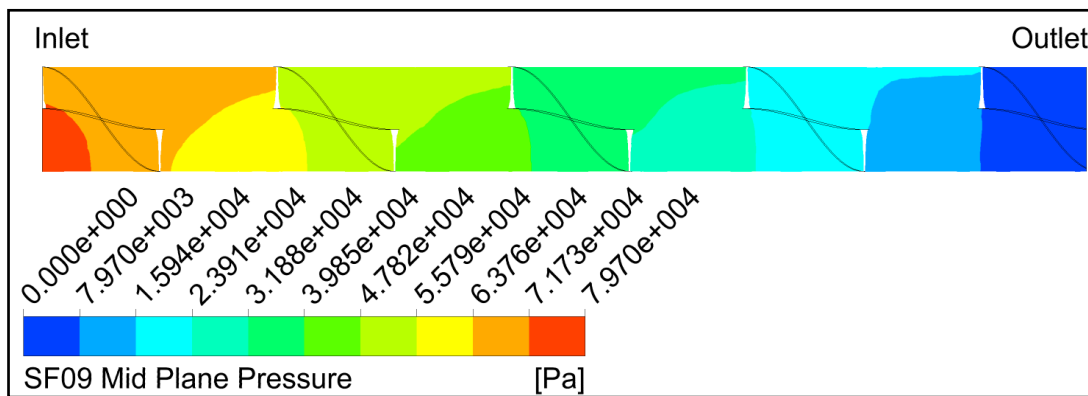

Figure B.27: Pressure drop along the mid plane of model SF08.

Results SF10

The results presented here are for filter model SF10 which has no baffle. This model was used as a abase line for some of the comparisions made in the results section of the dissertation.

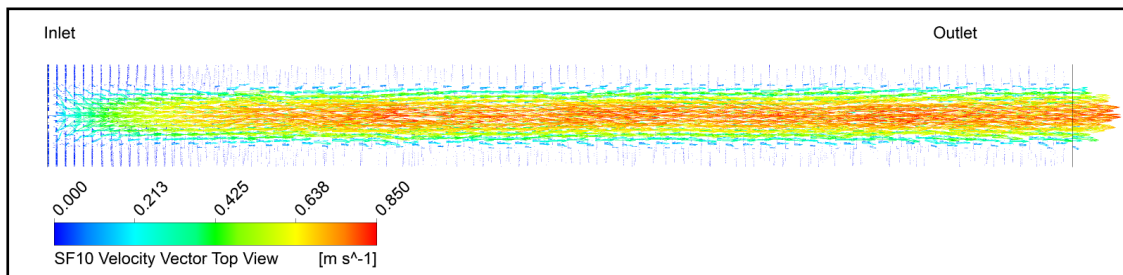The dimensions of the filter model SF10 are identical to that of the other filters; 0.2m diameter and 2m length.

Figure B.28: Velocity vectors shown from the top of the filter SF10.

Velocity vectors in SF10 viewed from the side show the effects of water channelling of the flow through the filter.
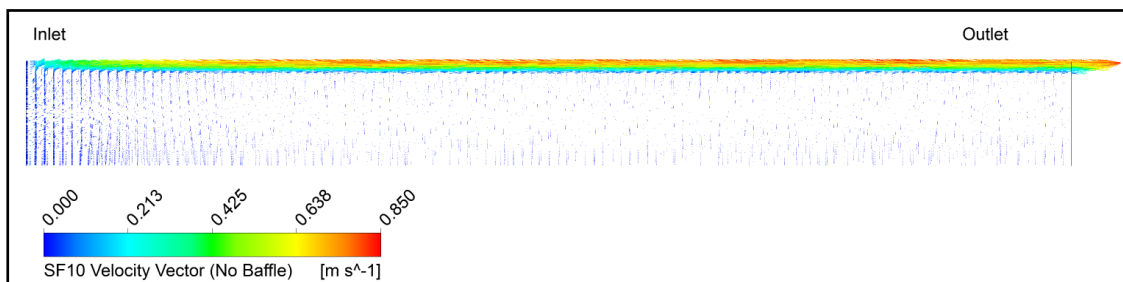

Figure B.29: Velocity vectors projected onto mid plane of filter SF10.

The pressure drop is less than the other filters due to the absence of baffles which cause restriction to the flow.
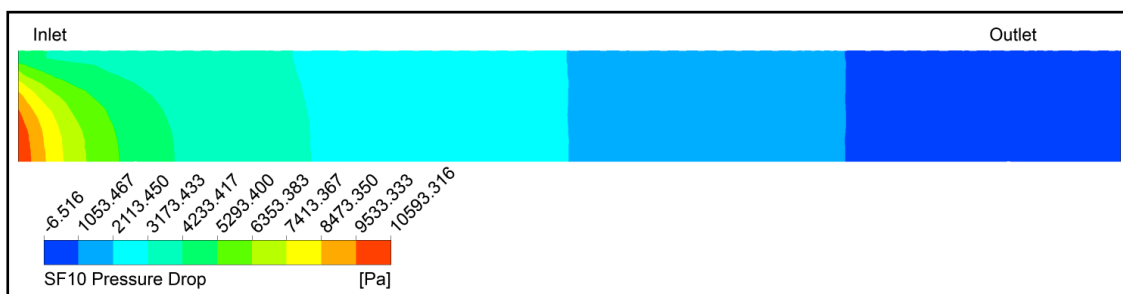

Figure B.30: Pressure drop across filter SF10.

Appendix C – Water Channel User Defined Function (UDF)

The code below has been written in 'C' programming language and is designed to work within ANSYS Fluent™. The purpose of the code is to set viscous resistance values in each axis to simulate an area of low resistance along the top of a horizontal sand filter.

For further details on the creation of UDF's refer to ANSYS Fluent UDF manual available from help menu within the software.

```c
/* Viscous Resistance Profile UDF in a Porous Zone*/
/* Sets the viscous resistance in the top 5% of the filter */
/* to 1e9 by using the height in the Y axis to the chord of*/
/* the semicircular area of the filter. The center cross section*/
/* of the filter must be constructed around the axis*/

#include "udf.h"

DEFINE_PROFILE(vis_res_1,t,i)
{
        real y[ND_ND];
        real a;
        cell_t c;
        begin_c_loop(c,t)
          {
                C_CENTROID(y,c,t);
                if( y[1] < 0.081196)
                  a = 4.89e9;
                else
                  a = 4.89e6;
                F_PROFILE(c,t,i) = a;
          }
        end_c_loop(c,t)
          }
```

References

AIAA 1998, Guide for the Verification and Validation of Computational Fluid Dynamics Simulations (AIAA-G-077-1998), AIAA Standards, American Institute of Aeronautics and Astronautics.

ANSYS FLUENT User's Guide, 2010, 13 edn, ANSYS, Inc, Canonsburg, PA.

Binnie, C, Smethurst, G, Kimber, M & Open University. 2002, *Basic water treatment*, 3rd edn, Thomas Telford; IWA publishing, London.

Horvath, I 1994, *Hydraulics in water and waste-water treatment technology*, Wiley, Budapest, New York.

Ingallinella, AM, Wegelin, M & Stecca, LM 1998, 'Up-flow roughing filtration: rehabilitation of a water treatment plant in Tarata, Bolivia', *Water Science & Technology*, vol. 37, no. 9, p. 105 EBSCOhost, a9h item: 8405541

Mead, S 2009, 'Numerical Modelling of Horizontal Flow in Sand Filters', Dissertation thesis, University of Southern Queensland.

Mossad, R & Aral, H 2010, 'Numerical Modeling of Flow in a Horizontal Sand Filter', *American Journal of Engineering & Applied Sciences*, vol. 3, no. 2, pp. 286-92

Salazar-Mendoza, R & Espinosa-Paredes, G 2009, 'A Three-Region Hydraulic Model for Solid-Liquid Flow with a Stationary Bed in Horizontal Wellbores', *Petroleum Science & Technology*, vol. 27, no. 10, pp. 1033-43 EBSCOhost, a9h item: 39768863

Scheidegger, AE 1963, *The physics of flow through porous media*, Oxford University Press, London.

Skouras, ED, Burganos, VN, Paraskeva, CA & Payatakes, AC 2007, 'Simulation of the dynamic behavior of horizontal granular filters', *Separation & Purification Technology*, vol. 56, no. 3, pp. 325-39 EBSCOhost, a9h item: 26038992

Suliman, F, Futsaether, C, Oxaal, U, Haugen, LE & Jenssen, P 2006, 'Effect of the inlet–outlet positions on the hydraulic performance of horizontal subsurface-flow wetlands constructed

with heterogeneous porous media', *Journal of Contaminant Hydrology*, vol. 87, no. 1/2, pp. 22-36 EBSCOhost, a9h item: 22081807

Tu, J, Yeoh, G, Heng & Liu, C 2008, *Computational Fluid Dynamics, A Practical Approach*, Elsevier, Oxford.

Zhao, C 2011, 'Grading Limit Determination for Channeling Paths and Particle Size Calculation for Plugging Agents', *Petroleum Science & Technology*, vol. 29, no. 5, pp. 506-13 EBSCOhost, a9h item: 57378320